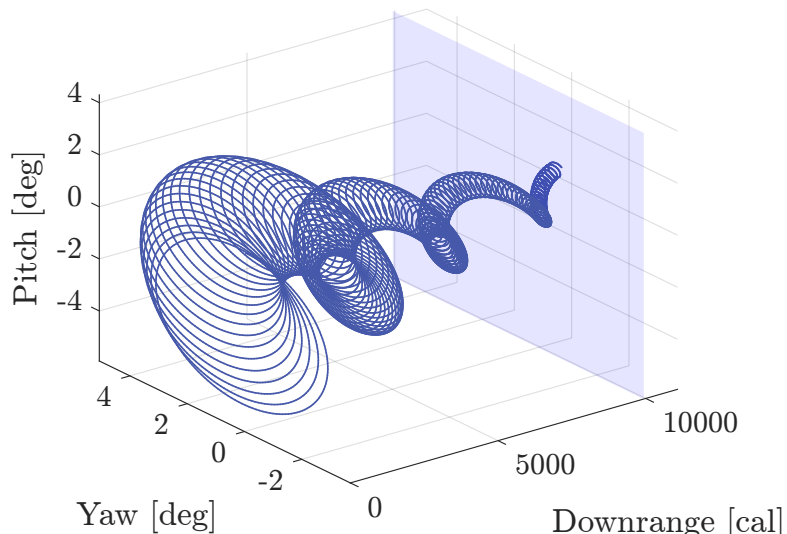


POLITECNICO
MILANO 1863

Projectiles Gyroscopic and Dynamic Stability



Submitted By,

Nicolò Lontani
10680453

Corso di Fondamenti di Balistica ed Esplosivistica
School of Industrial Engineering
Academic Year 2023-2024

Abstract

This report applies the "**Linearized Theory of Spin-Stabilized Projectiles**" to study the gyroscopic and dynamic stability of projectiles. Unlike the more computationally costly 6 Degrees of Freedom (DOFs) model, the study emphasizes computational economy by deriving and using closed-form analytical solutions for the projectile gyroscopic motion. The report focuses on the concepts of gyroscopic and dynamic stability and their dependency on projectile design parameters. The components of lateral deflection due to the gyroscopic motion (Aerodynamic Jump, Lateral Throw-off, and Gyroscopic Drift) are explained. The `bulletStability` code, developed in MATLAB® especially for this purpose, has been used to analyze the varied gyroscopic motions of different projectiles. The correctness and usefulness of the linearized theory for assessing and enhancing projectile stability and ballistic performance are demonstrated by comparing simulation results with Miller's formula.

$$S_d = \frac{2 \left(C_{L_\alpha} + \frac{md^2}{I_x} C_{M_{p\alpha}} \right)}{C_{L_\alpha} - C_D - \frac{md^2}{I_y} (C_{M_q} + C_{M_{\dot{\alpha}}})} \quad (1)$$

List of symbols

C_D	Aerodynamic Drag Coefficient	β	Sideslip angle / Yaw angle
$C_{L\alpha}$	Lift coefficient derivative w.r.t. angle of attack	ξ	Complex yaw
$C_{M\alpha}$	Overturning moment coefficient derivative w.r.t. angle of attack	φ	Aerodynamic roll angle
$C_{M_{p\alpha}}$	Magnus moment coefficient	Ma	Mach Number
C_{M_q}	Damping in pitch coefficient	p	Roll Rate
$C_{M_{\dot{\alpha}}}$	Pitching moment coefficient derivative w.r.t. the time derivative of α	q	Pitch Rate
C_{l_p}	Damping in roll coefficient	θ	Azimuth angle
d	Projectile diameter, caliber	ϕ	Elevation angle
V	Linear velocity	I_x	Moment of inertia around roll axis
g	Acceleration due to gravity	I_y	Moment of inertia around transversal axis
S	Reference surface, computed with d	T	Air temperature
S_g	Gyroscopic stability factor	ρ	Air density
S_d	Dynamic stability factor	m	Projectile mass
α	Angle of Attack / Pitch angle	ε	Dynamic unbalance angle/in-bore yaw
		$\hat{\varepsilon}$	Static unbalance

Contents

1	Linearized Theory for Spin-Stabilized Projectiles	1
1.1	Introduction	1
1.2	Assumptions and Coordinate Systems	2
1.3	Linearized Equations of Motion	4
1.3.1	Important Remarks	6
2	Epicycle Motion of Spinning Projectile	7
2.1	Simplified Epicyclic motion of spinning projectiles	7
2.1.1	Classical Gyroscopic Stability Criterion	8
2.2	Complete Epicyclic motion of spinning projectile	9
2.2.1	Dynamic and Gyroscopic Stability Relation	10
2.2.2	Gyroscopic Stability Dependencies	11
2.3	Initial Conditions	12
2.4	Lateral Deflection	13
2.4.1	Aerodynamic Jump	14
2.4.2	Lateral Throw-off	14
2.4.3	Gyroscopic Drift	15
3	bulletStability Code	16
3.1	Governing Equations and Code Diagram	16
3.2	9x19mm Parabellum	18
3.3	9x39mm SP-5 Subsonic Bullet	22
3.4	7mm Bullet	25
3.5	Comparison with Miller's Formula	29
4	Conclusions	31
A	Derivation Process for the Equations of Motion	33
A.0.1	Linear Velocity Equation of Motion	34
A.0.2	Roll Equation of Motion	34
A.0.3	Linearized Yawing and Pitching Equation of Motion	35
B	Equations used in bulletStability code	37
C	Results from the simulations	38

List of Figures

1.1	Projectile geometric sections	2
1.2	Fixed and Non-rolling coordinate system	3
1.3	Non-rolling and Body coordinate system	3
1.4	Two sets of equivalent aerodynamic angles	4
2.1	Epicyclic motion described by Equation 2.2.	8
2.2	Relation between dynamic stability factor and gyroscopic stability factor	10
2.3	Magnus effect schematization. A clockwise rotating cylinder immersed in a left-to-right flow experiences a vertical force that points up. This effect is the cause of the Aerodynamic Jump component of deflection.	14
3.1	Block diagram that schematize the bulletStability code	17
3.2	9x19mm Parabellum 124 grains geometry	18
3.3	9x19mm Parabellum 158 grains geometry	18
3.4	3D epicycle trajectory of 9x19mm Parabellum 124gr. The blue plane identifies the transition from transonic to subsonic regime.	19
3.5	3D epicycle trajectory of 9x19mm Parabellum 158gr. The blue plane identifies the transition from transonic to subsonic regime.	19
3.6	9x19mm Parabellum 124gr epicycle trajectory from the muzzle perspective . . .	20
3.7	9x19mm Parabellum 158gr epicycle trajectory from the muzzle perspective . . .	20
3.8	Mach number, aerodynamic drag coefficient and lift coefficient derivative during flight of 9x19 Parabellum 124gr and 158gr respectevely	21
3.9	Stability diagram for 9x19 Parabellum bullets weighting 124gr and 158gr. The evolution of the point in the diagram goes from the darkest to the lightest color.	21
3.10	9x19mm Parabellum 124gr deflection components: Aerodynamic Jump and Lateral Throw-off deflection with respect of rifling twist rate. On the right Gyroscopic Drift vs Downrange.	22
3.11	9x19mm Parabellum 124gr deflection components: Aerodynamic Jump and Lateral Throw-off deflection with respect of rifling twist rate. On the right Gyroscopic Drift vs Downrange.	22
3.12	9x39mm SP-5 geometry	23
3.13	3D epicycle trajectory of 9x39mm SP-5. The blue plane identifies the transition from transonic to subsonic regime.	23
3.14	9x39mm SP-5 epicycle trajectory from the muzzle perspective.	24
3.15	Mach number, aerodynamic drag coefficient and lift coefficient derivative during flight of 9x39mm SP-5.	24
3.16	Stability diagram for 9x39mm SP-5. The evolution of the point in the diagram goes from the darkest to the lightest color.	24
3.17	Epicycle trajectory and stability diagram for a 9x39mm with higher damping in roll. The evolution of the point in the diagram goes from the darkest to the lightest color.	25
3.18	9x39mm SP-5 deflection components: Aerodynamic Jump and Lateral Throw-off deflection with respect of rifling twist rate. On the right Gyroscopic Drift vs Downrange.	25
3.19	7mm hunting bullet geometry	26

3.20	3D epicycle trajectory of 7mm bullet.	26
3.21	7mm epicycle trajectory from the muzzle perspective	26
3.22	Mach number, aerodynamic drag coefficient and lift coefficient derivative during flight of the 7mm bullet.	27
3.23	Stability diagram for the 7mm bullet. The evolution of the point in the diagram goes from the darkest to the lightest color.	27
3.24	7mm bullet deflection components: Aerodynamic Jump and Lateral Throw-off deflection with respect of rifling twist rate. On the right Gyroscopic Drift vs Downrange.	27
3.25	7mm bullet fired from different rifling twist rate. The grey plane represents the downrange value for which the bullet enters the transonic regime, which in this case is of $\approx 960m$	28
3.26	(a) showing all the previous trajectories of the 7mm shot by different riflings. Figure (b) is a detail of Figure (a).	28
3.27	7mm epicycle trajectory from the muzzle perspective	29

List of Tables

2.1	Quantities influencing the gyroscopic stability factor S_g	11
3.1	Comparison between the twist rate, in calibers/turn, resulting from Miller's formula and the twist rate needed for marginal stability resulting from the Linearized Theory	30
C.1	Initial conditions and results for the 9x19mm Parabellum 124gr	38
C.2	Initial conditions and results for the 9x19mm Parabellum 158gr	38
C.3	Initial conditions and results for 9x39mm SP-5 subsonic bullet	39
C.4	Initial conditions and results for 7mm bullet	39

Chapter 1

Linearized Theory for Spin-Stabilized Projectiles

1.1 Introduction

In the field of bullets and projectiles flight simulations the most accurate and complex model is the 6 Degrees of Freedom (DOFs) model. Through this model, the trajectory is calculated by integrating the nonlinear equations of motion through numerical schemes. This does not only imply a fair amount of computational cost (which leads to longer computational times), but it also need the most detailed aerodynamic characterization of the projectile out of all models. Characterizing the aerodynamics of a projectile is not easy, and can be done either through wind tunnel experiments, Computation Fluid Dynamics (CFD) simulations or semi-empirical component build-up softwares.

However, if we are merely interested in analysing the stability of projectiles, it is possible to develop a theory through various simplifications which leads to analytic formulas describing the gyroscopic motions and the lateral deflection due to it. This allows us to use only the main aerodynamic coefficients, which are the easier ones to estimate. Since we have closed formulas instead of differential equations, computations are significantly faster, and during history it was tested that the difference in accuracy between the two models is surprisingly small. Matter of fact, the results that comes from this linearized theory are now used to estimate some of the aerodynamic coefficients by measuring the projectile attitude at various stations of the flight during shooting experiments. Another reason why this linear theory is valuable is that we can directly see, through the analytical results, what quantities affect stability during flight. This is important in the design process of projectiles, when we have to make choices to improve various ballistic performances for both external and terminal ballistics. The best work on this theory is developed in the "**Modern Exterior Ballistics**"[1] book by Robert L.McCoy, which has served as the basis for all other major external ballistics books and articles on the subject.

In this report we are gonna:

- Show the derivation process and the results of the Linearized Theory for Spin-Stabilized Projectiles
- Introduce and explain the concept of gyroscopic and dynamic stability
- Explain the components of deflection caused by the gyroscopic motion
- Analyse real bullets through the `bulletStability` code written in MATLAB ®
- Compare the results from this theory with Miller's formula for gyroscopic stability.

1.2 Assumptions and Coordinate Systems

Projectiles are bodies of revolution, therefore they are symmetric about an axis, which in this report is always considered to be the x-axis. In general, every projectile is geometrically composed of

- An ogive, the curved section at the front, which is also commonly called "nose". Its purpose in external ballistics is primarily to reduce drag, but it also has several effects on flight stability
- A cylindrical section
- A boat tail, the tapered section at the end. Its main purpose is to reduce drag and only certain projectile features it, typically rifle bullets.

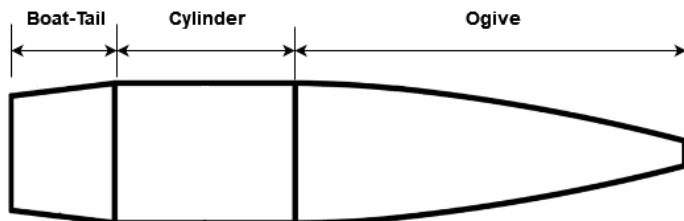


Figure 1.1: Projectile geometric sections

In this report, unless otherwise stated, the projectiles are considered to be geometrically perfect and composed of a single homogeneous material. Given these assumptions, the center of mass will lie on the axis of symmetry.

To accurately represent the direction of the vectorial quantities in the computations we need to define three coordinate systems:

- $[\vec{I}, \vec{J}, \vec{K}]$, triad fixed to the ground;
- $[\vec{i}, \vec{j}, \vec{k}]$, Non-rolling triad, attached to the projectile center of mass. The unit vector \vec{i} is always tangent to the trajectory;
- $[\vec{x}, \vec{y}, \vec{z}]$, triad of the body reference system. It is attached to the bullet center of mass and it rotates with the body. \vec{x} is always directed as the axis of symmetry of the body.

These triads and the relationship between them are graphically shown in Figure 1.2 and Figure 1.3. The angles that relate the Fixed triad with the Non-rolling one are the **azimuth** θ and the **elevation** ϕ , while the angles that relate the Non-rolling triad with the Body one are the **total angle of attack** α_{tot} and the **roll angle** φ .

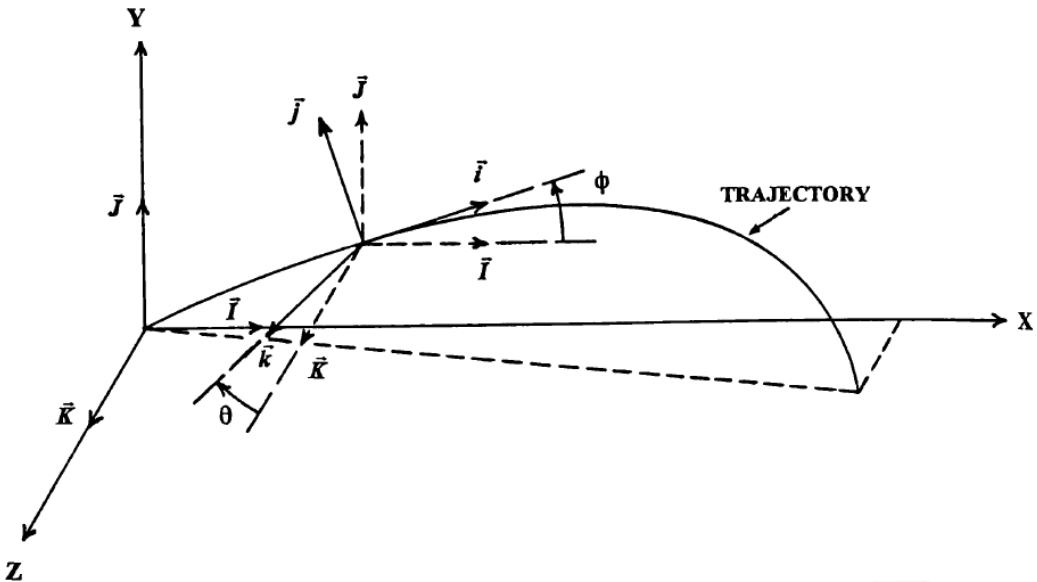


Figure 1.2: Fixed and Non-rolling coordinate system

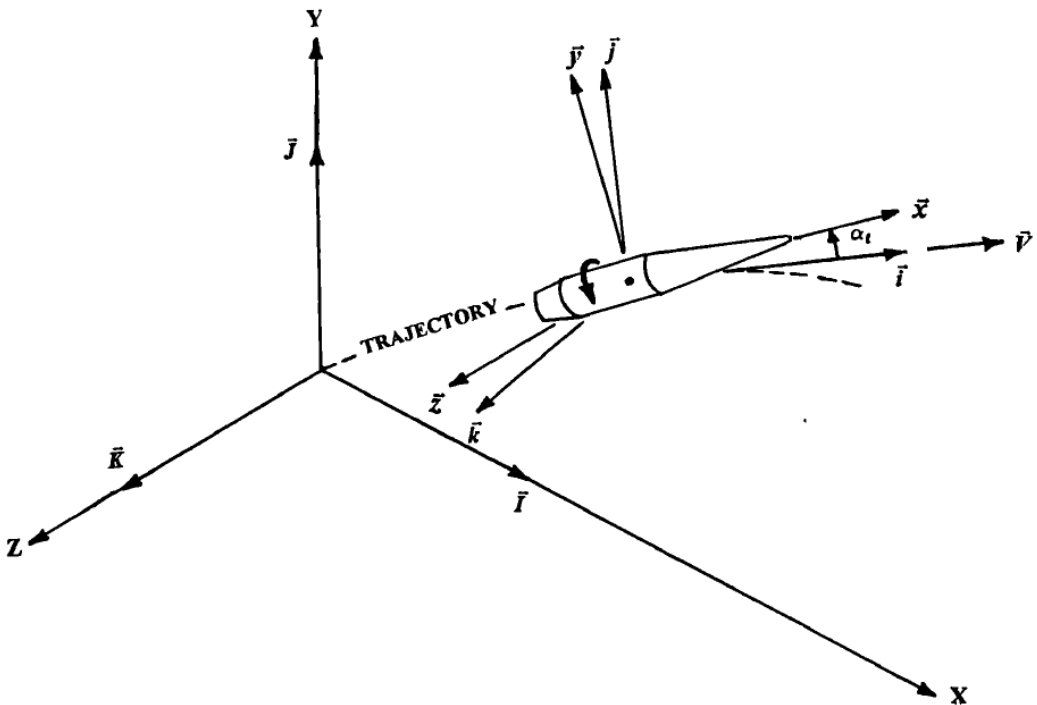


Figure 1.3: Non-rolling and Body coordinate system

Remark: in this linearized framework α_{tot} is the angle that the x-axis of the body forms with the velocity vector. It is usually called "yaw" in ballistics, since the projectiles are axial-symmetric. In this framework, however, we define as "yaw" the angle β (which is the aerodynamic angle in the $\vec{i} - \vec{k}$ plane) and as "pitch" the angle α (which is the aerodynamic angle in the $\vec{i} - \vec{j}$ plane). These two angles are completely equivalent to the α_{tot} and φ set of angles. The reason why this is handy is that with the set α and β we can easily describe the gyroscopic motion, while α_{tot} describes the total magnitude of the aerodynamic angle that the projectile experiences. Given this considerations $\alpha_{tot} = \sqrt{\alpha^2 + \beta^2}$. Figure 1.4 denotes the equivalence between the two sets of aerodynamic angles.

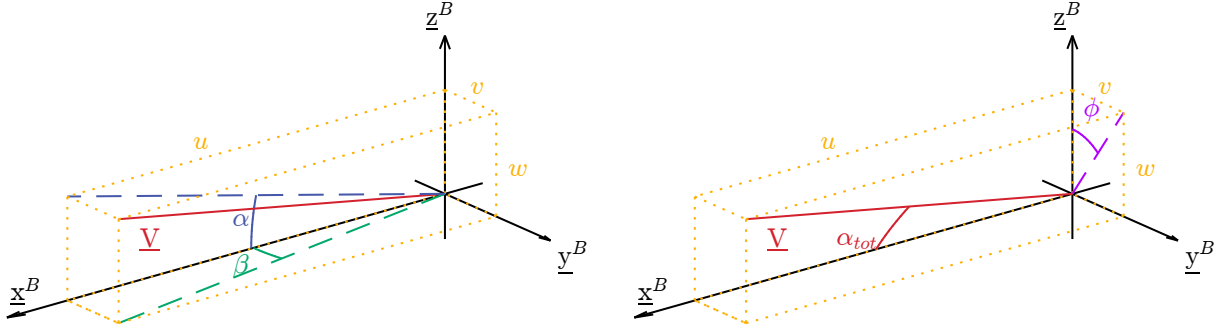


Figure 1.4: Two sets of equivalent aerodynamic angles

It is possible to pass from $[\vec{I}, \vec{J}, \vec{K}]$ to $[\vec{i}, \vec{j}, \vec{k}]$ and vice versa through the following Eulerian angular relationships:

$$\vec{i} = \cos \phi \cos \theta \vec{I} + \sin \phi \cos \theta \vec{J} + \sin \theta \vec{K} \quad (1.1)$$

$$\vec{j} = -\sin \phi \vec{I} + \cos \phi \vec{J} \quad (1.2)$$

$$\vec{k} = -\cos \phi \sin \theta \vec{I} - \sin \phi \sin \theta \vec{J} + \cos \theta \vec{K} \quad (1.3)$$

$$\vec{I} = \cos \phi \cos \theta \vec{i} - \sin \phi \vec{j} - \cos \phi \sin \theta \vec{k} \quad (1.4)$$

$$\vec{J} = \sin \phi \cos \theta \vec{i} + \cos \phi \vec{j} - \sin \phi \sin \theta \vec{k} \quad (1.5)$$

$$\vec{K} = \sin \theta \vec{i} + \cos \theta \vec{k} \quad (1.6)$$

1.3 Linearized Equations of Motion

The 6 equations of motion express the behaviour of the projectile, considered as a rigid body, with respect to time. In our case, from the equations we can drop the rocket forces because the bodies considered in the analysis do not produce thrust. We can also neglect the Coriolis acceleration because it can be considered small in comparison to the acceleration due to gravity. The equations expressed in vector form are:

$$m \frac{d\vec{V}}{dt} = \Sigma \vec{F} + m\vec{g} \quad (1.7)$$

$$\frac{d\vec{H}}{dt} = \Sigma \vec{M} \quad (1.8)$$

Where V is the linear velocity, F and M represents the aerodynamic force and moment components, m is the mass of the projectile, g is the acceleration due to gravity and H is the angular momentum.

In this framework, only those components of aerodynamic force and momentum that most affect stability will be retained, the choice of which is primarily supported by experimental

data. They can be expressed as:

$$\text{Drag Force} = -\frac{1}{2}\rho SC_D V^2 \vec{i} \quad (1.9)$$

$$\text{Lift Force} = -\frac{1}{2}\rho SC_{L_\alpha} V^2 [\vec{i} \times (\vec{x} \times \vec{i})] \quad (1.10)$$

$$\text{Spin Damping Moment} = \frac{1}{2}\rho SdV^2 \left(\frac{pd}{V}\right) C_{l_p} \vec{x} \quad (1.11)$$

$$\text{Overturning Moment} = \frac{1}{2}\rho SdC_{M_\alpha} V^2 (\vec{i} \times \vec{x}) \quad (1.12)$$

$$\text{Magnus Moment} = \frac{1}{2}\rho SdV^2 \left(\frac{pd}{V}\right) C_{M_{p\alpha}} [\vec{x} \times (\vec{i} \times \vec{x})] \quad (1.13)$$

$$\text{Pitch Damping Moment} = \frac{1}{2}\rho Sd^2 C_{M_q} V \left(\vec{x} \times \frac{d\vec{x}}{dt}\right) + \quad (1.14)$$

$$+ \frac{1}{2}\rho Sd^2 C_{M_\alpha} V \left[\left(\vec{x} \times \frac{d\vec{x}}{dt}\right) - \left(\vec{x} \times \frac{d\vec{i}}{dt}\right)\right] \quad (1.15)$$

In this linearized framework are often used two conventions that work particularly well together. The first one is the "starred convention", developed by C.H.Murphy, that defines "starred coefficients" as

$$C_x^* = \frac{\rho Sd}{2m} C_x \quad (1.16)$$

where C_x is a generic aerodynamic coefficient. This convention is really useful when used alongside equations where the independent variable is the dimensionless distance s (in calibers). This change of variable from time to dimensionless distance allows for a better study of stability, since bullets and projectiles with very different dimensions will have the same period of yaw measured in calibers. The dimensionless distance is defined as such:

$$s = \frac{1}{d} \int_0^t V dt \quad (1.17)$$

Note that in this report the derivative with respect to time is indicated by the symbol " \dot{Q} " and the derivative with respect to dimensionless distance by the symbol " Q'' ", with Q being any quantity. All the following equations of motion will be written with s as the independent variable.

For the sake of reading convenience, the derivation process of the Linearized Equations of Motion is shown in Appendix A. Following are listed only the resulting equations that will be used for flight stability analysis:

Linear Velocity Equation

$$V = V_0 e^{\int_0^s -C_D^* ds} \quad (1.18)$$

Roll Rate or Axial Spin Equation

$$p = \frac{V}{d} \left(\frac{pd}{V} \right)_0 e^{-K_p s} \quad (1.19)$$

where

$$K_p = -[k_x^{-2} C_{l_p}^* + C_D^*]$$

$$k_x^{-2} = \frac{md^2}{I_x}$$

Yaw and Pitch Equation

$$\xi'' + (H - iP) \xi' - (M + iPT) \xi = -iPG \quad (1.20)$$

where

$$\xi = \alpha + i\beta$$

$$H = C_{L_\alpha}^* - C_D^* - k_y^{-2} (C_{M_q}^* + C_{M_\alpha}^*)$$

$$P = \left(\frac{I_x}{I_y} \right) \left(\frac{pd}{V} \right)$$

$$M = k_y^{-2} C_{M_\alpha}^*$$

$$T = C_{L_\alpha}^* + k_x^{-2} C_{M_{p\alpha}}^*$$

$$G = \frac{gd \cos \phi}{V^2}$$

$$k_x^{-2} = \frac{md^2}{I_x}$$

$$k_y^{-2} = \frac{md^2}{I_y}$$

1.3.1 Important Remarks

Equation 1.18 shows us how velocity decreases during flight. If we assume that the coefficient of drag C_D remains constant during flight, which is a good approximation for highly supersonic or subsonic bullets, the expression simplifies to:

$$V = V_0 e^{-C_D^* ds} \quad (1.21)$$

which tells us that the velocity of a projectile decreases exponentially while travelling down-range. The value of C_D^* is of great impact, and even a slight increase in value leads to considerable change in linear acceleration.

Looking at Equation 1.19 we can see a similar trend. However in this case the exponent is positive, since for spin-stabilized projectiles K_p is usually a negative number. This means that the **quantity pd/V increases during the flight of the projectile**. This quantity is measured in radians per caliber of travel, therefore is a measure of how much the projectile spins relative to the amount of distance it travels. In short, this tells us that **the linear velocity V decreases faster than the roll rate p** , which is a remarkable result for flight stability and will be investigate more thoroughly in the next chapters.

Chapter 2

Epicycle Motion of Spinning Projectile

2.1 Simplified Epicyclic motion of spinning projectiles

Before diving into the solution of Equation 1.20, we will study a simpler formulation, that is fundamental for the introduction of the gyroscopic stability concept. By retaining only the pitching moment and the gravitational contributions we get the following simplified expression:

$$\xi'' - iP\xi' - M\xi = -iPG \quad (2.1)$$

This is a linear second-order differential equation with complex coefficients, which solution is:

$$\xi = K_F e^{i\phi_F} + K_S e^{i\phi_S} + i\beta_R \quad (2.2)$$

where

K_F is the amplitude of the fast epicyclic mode arm

K_S is the amplitude of the slow epicyclic mode arm

$\phi_F = \phi_{F0} + \phi'_F s$

$\phi_S = \phi_{S0} + \phi'_S s$

ϕ_{F0} is the initial phase angle of the fast epicyclic mode arm

ϕ_{S0} is the initial phase angle of the slow epicyclic mode arm

$\phi'_F = \frac{1}{2} [P + \sqrt{P^2 - 4M}]$ the fast mode arm turning rate

$\phi'_S = \frac{1}{2} [P - \sqrt{P^2 - 4M}]$ the slow mode arm turning rate

$\beta_R = \frac{PG}{M}$

Equation 2.2 is of great physical interest, it shows that the pitching and yawing motion consists of two modes, a slow mode (called precession) and a fast mode (called nutation). The spin-stabilized projectile acts as a gyroscope. It can be noticed that if the quantity $(P^2 - 4M)$ is positive, the exponents of the two modes are purely imaginary. If no exponent contains a real part, the magnitude of the slow and fast modes arms remain fixed, describing an **undamped epicyclic pitching and yawing motion**.

The third term comes from the particular solution of Equation 2.1, and corresponds to the yaw of repose β_R . The yaw of repose is caused by the interaction of the roll rate with the acceleration of gravity. Let's imagine a flat-fire trajectory: when gravity pulls the projectile down, the projectile wants to retain its attitude in space, because it acts like a gyroscope. It will therefore develop an aerodynamic angle between its axis of rotation and the direction of the velocity vector. In this situation a pitching moment develops, creating a torque τ . Euler's second law $\frac{d\vec{L}}{dt} = \vec{\tau}$ states that the angular momentum vector \vec{L} tries to align itself with the direction of the torque τ , therefore the projectile tends to point a bit to the right or left (depending on the spin direction) creating the angle β_R . The yaw of repose is usually of order $[10^{-3}]$ degrees, which is small compared to usual total angles of attack α_{tot} at the start of the trajectory. The importance of the estimate of β_R is in the field of trajectory drift: even if its

magnitude is small, it produces non-negligible effects because it is an aerodynamic angle that persists for the whole flight of the projectile.

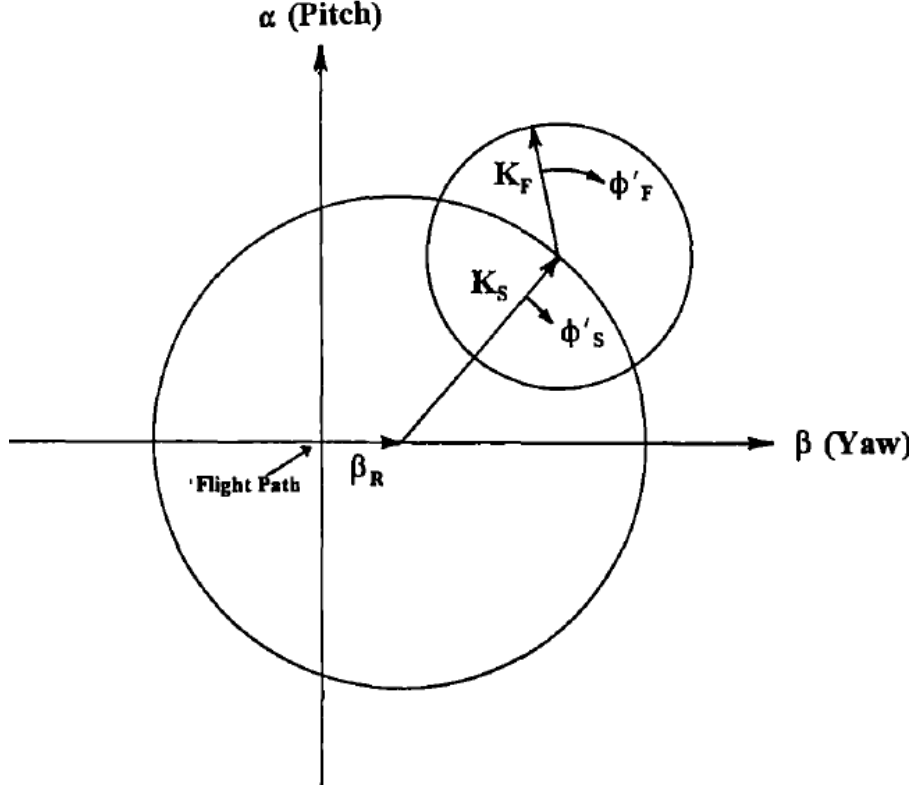


Figure 2.1: Epicyclic motion described by Equation 2.2.

2.1.1 Classical Gyroscopic Stability Criterion

Gyroscopic stability is a crucial concept in external ballistics for spin-stabilized projectiles. This concept is used to ensure that the projectile begins its trajectory without immediately tumbling in front of the barrel. The theory comes directly from the previous observation about the quantity $(P^2 - 4M)$. If this quantity would be negative, the exponents of the two modes will have a real part. Since one of these two real components would be positive, it means that the mode associated will increase in magnitude indefinitely, leading to an unstable motion.

A projectile is therefore considered gyroscopically stable if this does not happen, namely if

$$(P^2 - 4M) > 0 \quad (2.3)$$

The concept of gyroscopic stability factor S_g comes naturally from it

$$S_g = \frac{P^2}{4M} = \frac{I_x^2 p^2}{2\rho I_y S d V^2 C_{M_\alpha}} \quad (2.4)$$

The higher the value of S_g , the more the projectile is gyroscopically stable. By writing Equation 2.4 with respect to P^2 and substituting in Equation 2.3 we get

$$4M(S_g - 1) > 0 \quad (2.5)$$

which leads to the classical gyroscopic stability criteria for spin stabilized bullets:

$$S_g > 1 \quad (2.6)$$

As previously stated in subsection 1.3.1, during the flight of a projectile the linear velocity V decreases in magnitude faster than the roll rate p . From Equation 2.4 it can be noted that $S_g \propto p^2/V^2$. This means that the first portion of the flight is the most critical one, because it is the section in which p^2/V^2 is higher and the projectile is less gyroscopically stable. As we will see more in depth at the end of section 3.4, this is not the only section of the flight where instability can occur. In reality the coefficients affecting flight stability can change a lot depending on the Mach regime, causing a shift in the balancing forces that in the worst case scenario can end up in instability or loss in accuracy.

2.2 Complete Epicyclic motion of spinning projectile

Now that we have introduced the concept of gyroscopic stability we can return to the full yaw-pitch linearized equation of motion:

$$\xi'' + (H - iP)\xi' - (M + iP\Gamma)\xi = -iPG \quad (2.7)$$

Solving this equation we get the same solution shape of Equation 2.2

$$\xi = K_F e^{i\phi_F} + K_S e^{i\phi_S} + i\beta_R \quad (2.8)$$

but with the following coefficients:

$$K_F = K_{F_0} e^{\lambda_{F^s}} \quad (2.9)$$

$$K_S = K_{S_0} e^{\lambda_{S^s}} \quad (2.10)$$

$$\phi_F = \phi_{F_0} + \phi'_F \quad (2.11)$$

$$\phi_S = \phi_{S_0} + \phi'_S \quad (2.12)$$

$$\beta_R = \frac{PG}{M + iP\Gamma} \quad (2.13)$$

$$\lambda_F + i\phi'_F = \frac{1}{2} \left[-H + iP + \sqrt{4M + H^2 - P^2 + 2iP(2T - H)} \right] \quad (2.14)$$

$$\lambda_S + i\phi'_S = \frac{1}{2} \left[-H + iP - \sqrt{4M + H^2 - P^2 + 2iP(2T - H)} \right] \quad (2.15)$$

This solution is completely analogous to the previously analized solution of Equation 2.1, hence it describes the same type of epicyclic motion, but now the exponents of the two modes have real parts. The solution results in a **damped epicycle motion**, which can be stable or unstable depending on the signs of λ_F and λ_S .

The values of λ_F , λ_S , ϕ'_F and ϕ'_S are obtained through a series of algebraic computations:

$$\phi'_F = \frac{1}{2} \left[P + \sqrt{P^2 - 4M} \right] \quad (2.16)$$

$$\phi'_S = \frac{1}{2} \left[P - \sqrt{P^2 - 4M} \right] \quad (2.17)$$

$$\lambda_F = -\frac{1}{2} \left[H - \frac{P(2T - H)}{\sqrt{P^2 - 4M}} \right] \quad (2.18)$$

$$\lambda_S = -\frac{1}{2} \left[H + \frac{P(2T - H)}{\sqrt{P^2 - 4M}} \right] \quad (2.19)$$

Since the expressions of ϕ'_F and ϕ'_S are the same as the ones in section 2.1, the definition of gyroscopic stability and gyroscopic stability factor S_g still apply to this case.

2.2.1 Dynamic and Gyroscopic Stability Relation

The dynamic stability behavior of the motion depends on the signs of λ_F and λ_S . A projectile is dynamically stable while flying if both of them are negative. From Equation 2.18 and Equation 2.19 it is possible to tell that both exponents are negative if the following criteria is met:

$$\left[H \mp \frac{P(2T - H)}{\sqrt{P^2 - 4M}} \right] > 0 \quad (2.20)$$

As we did for gyroscopic stability, we define a dynamic stability factor

$$S_d = \frac{2T}{H} \quad (2.21)$$

By substituting Equation 2.21 into Equation 2.20 we can write the relation between the gyroscopic stability and dynamic stability factors:

$$\frac{1}{S_g} = S_d (2 - S_d) \quad (2.22)$$

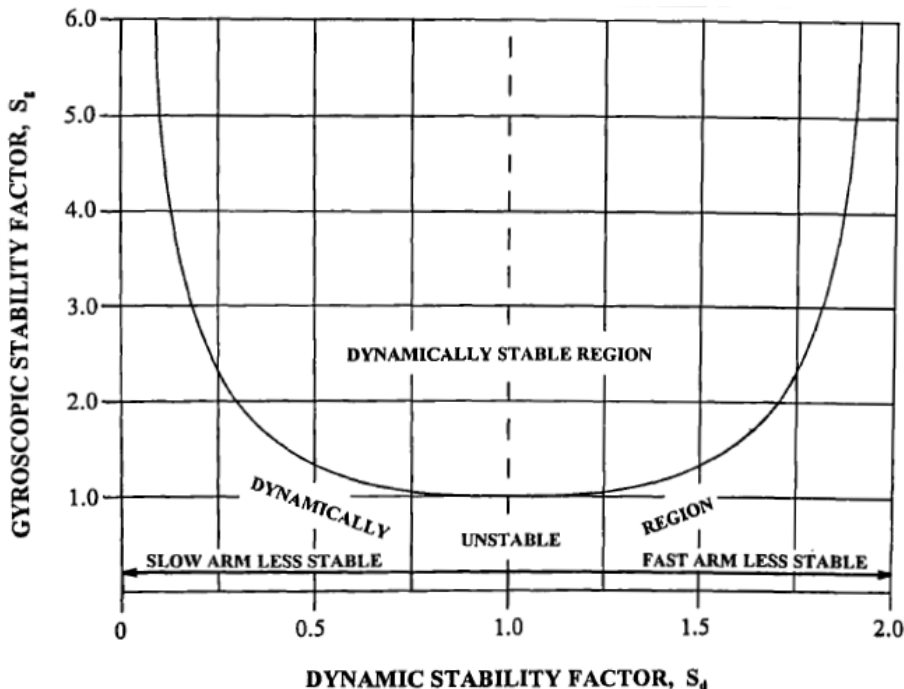


Figure 2.2: Relation between dynamic stability factor and gyroscopic stability factor

This relation is extremely important because from it we can compute the amount of roll rate/axial spin the projectile needs to be dynamically stable at the start of its trajectory. It is worth noting that the classical gyroscopic stability criterion stated previously as $S_g > 1$ is of relevant meaning only if $0.8 \lesssim S_d \lesssim 1.2$, as can be seen from Figure 2.2. Therefore from Equation 2.22 we state a more general gyroscopic stability criteria:

$$S_g > \frac{1}{S_d(2 - S_d)} \quad (2.23)$$

Generally speaking, it is better to design the rifling of the barrel to achieve marginal gyroscopic stability of fired bullets. The faster you spin a bullet, the less accurate it will be. There is no reason, linked to external ballistics, to spin a bullet any faster than the one necessary to

get the S_g that barely stabilizes the projectile. Another reason to not have over-stabilization is for "tractability": since the projectile is a gyroscope, it wants to retain its starting attitude instead of following the tangent of its trajectory. This can lead to high angles of attack for an over-stabilized bullet causing either dynamic instability or bad terminal performances.

Another consideration to be made is that if the bullet fired is dynamically unstable, $0 < S_d < 2$, no amount of axial spin is capable of stabilizing it.

2.2.2 Gyroscopic Stability Dependencies

Now that we know what is the meaning behind the gyroscopic stability factor S_g , it is interesting to state all the quantities that affect it and in which manner. These dependencies are illustrated in Table 2.1. It is essential to take into account what effect is associated with each choice made during the design process of a projectile. If this is not the case, an error can cause the projectile to be badly designed, causing loss in flight performance or, in the worst case scenario, divergence and tumbling during flight.

Table 2.1: Quantities influencing the gyroscopic stability factor S_g .

S_g dependencies	
Proportionality relation (\propto)	Description
I_x^2, I_y^{-1}, d^{-3}	For a given mass, changing the diameter of the projectile will increase all three quantities. In general, however, increasing the diameter results in a greater increase in I_y than in I_x . Moreover, the diameter appears at denominator with a cubic power. The conclusion is that, for a given roll rate p , an increase in diameter will decrease the gyroscopic stability. For a given muzzle speed, larger and longer projectiles require a faster rifling twist rate (more spin)
m	Let's make the assumption that the projectiles considered are made of a single homogeneous material. Usually, heavier projectiles of the same caliber are longer with respect to the lighter ones. But if we consider only a change in mass, due, for example, to a different material, then heavier bullets are more gyroscopically stable for the same amount of spin and speed . This is directly correlated to the fact that I_x and I_y are both linearly dependent to m , therefore from Equation 2.4 $S_g \propto m$.
p^2, V^{-2}	The proportionality between the spin and the gyroscopic stability factor is quadratic. An higher rifling twist rate increases the spin of the projectile, which make the projectile more stable. In reality, since S_g is also proportional to the V^{-2} , the important quantity to take into account is the ratio p/V . For a given spin, a faster bullet is less gyroscopically stable .
ρ^{-1}	Air density decreases with altitude. If we consider the temperature to be constant, the same projectile fired at an higher altitude will be more gyroscopically stable . This effect is usually marginal with respect to the others
$C_{M_\alpha}^{-1}$	The overturning moment coefficient is a difficult quantity to evaluate, but generally is directly proportional to the projectile length. This contribution adds to the reasons why for a given spin, a longer projectile is less gyroscopically stable .

2.3 Initial Conditions

The initial conditions that need to be set in order to compute the epicycle trajectory are the **complex initial yaw** ξ_0 and the **complex initial yaw-rate** ξ'_0 .

The initial amplitudes of the arms of the fast and slow modes, K_F and K_S , appearing in the solution of Equation 2.7, depend on the initial complex yaw ξ_0 and the initial complex yaw-rate ξ'_0 . By differentiating the expression of ξ from Equation 2.8 and evaluating it at the initial condition we get

$$\xi_0 = K_{F_0} e^{i\phi_{F_0}} + K_{S_0} e^{i\phi_{S_0}} \quad (2.24)$$

$$\xi'_0 = (\lambda_F + i\phi'_F) K_{F_0} e^{i\phi_{F_0}} + (\lambda_S + i\phi'_S) K_{S_0} e^{i\phi_{S_0}} \quad (2.25)$$

by manipulating the previous equations and neglecting the terms of higher order we get the dependence of the slow and fast modes arms with respect to the starting complex yaw ξ_0 and the starting complex yaw-rate ξ'_0 :

$$K_{F_0} e^{i\phi_{F_0}} = \left(\frac{i\xi'_0 + \phi'_S \xi_0}{\phi'_F - \phi'_S} \right) \quad (2.26)$$

$$K_{S_0} e^{i\phi_{S_0}} = \left(\frac{i\xi'_0 + \phi'_F \xi_0}{\phi'_F - \phi'_S} \right) \quad (2.27)$$

What remains to be defined is how to obtain the values of ξ_0 and ξ'_0 . Their values depend on some physical, geometrical and aerodynamic properties of the projectile that we need to properly define. Let's consider the mass distribution of a projectile: in the previous chapters we assumed that the projectile was perfectly axial-symmetric and that its center of gravity lies on its axis of symmetry. A projectile like such is obviously impossible to have in real life, or at least extremely difficult. Therefore, almost every projectile is statically unbalanced, and we can define the "**static unbalance**" as the radial distance between the center of gravity and the axis of symmetry; we denote it with the symbol $\hat{\varepsilon}$. In addition to being statically unbalanced, real projectiles have also some degree of **dynamic unbalance**, i.e. there is an angle between the principal axis of inertia related to spin and the axis of symmetry, called ε .

Even if the previous considerations are almost always true, we continue to consider a perfectly symmetric projectile both in shape and in mass distribution for consistency with the theory.

The fundamental consideration that allows us to compute ξ_0 and ξ'_0 is that **both static and dynamic unbalance are still present if the projectile enters the the rifling with an angle** (the projectile is "eccentrically engraved"). We make the following reasonable assumptions:

- the angle at which the projectile is inclined relative to the rifling does not change while it travel along the barrel
- the projectile travels along the barrel without "balloting", i.e. the projectile does not bounce from one groove to another
- the tilt occurs about the mid-point of the cylindrical section of the projectile

Given this assumptions the **dynamic unbalance angle** ε is exactly the angle at which the projectile enters the rifling. ε is therefore also referred to as **in-bore yaw**. This angle develops primarily because there is a space between the chamber and the start of the rifling, called freebore, where the bullet can tilt relative to the barrel. Another cause of in-bore yaw is a chamber misalignment with respect to the barrel.

The static unbalance $\hat{\varepsilon}$, on the other hand, depends on the position of the center of gravity with respect to the mid-point of the cylindrical section: if the center of gravity is ahead of the mid-point $\hat{\varepsilon}$ is positive, if it is behind $\hat{\varepsilon}$ negative.

Now we can easily express ξ_0 and ξ'_0 with respect to ε :

$$\xi_0 = \varepsilon e^{i\varphi_0} \quad (2.28)$$

$$\xi'_0 = i \left(\frac{pd}{V} \right) \varepsilon e^{i\varphi_0} \quad (2.29)$$

where φ_0 is the initial roll angle at the muzzle, defined as the angle between the vertically upward plane and the plane containing both the in-bore yaw and the bore axis (positive clockwise).

Unfortunately, the in-bore yaw is a difficult quantity to measure or estimate. A much easier quantity is the first maximum yaw angle δ_{max} that the projectile achieves during the first period of precession. The relation between δ_{max} and ε is a well known result in the Linear Theory for Spin-Stabilized Projectiles and it is referred to as "Kent's formula":

$$\sin \delta_{max} = \left(2 \frac{I_y}{I_x} - 1 \right) \left(\frac{\varepsilon}{\sqrt{1 - 1/S_g}} \right) \quad (2.30)$$

Therefore, starting from experimental data, it is possible to compute the in-bore yaw ε that gives the maximum δ_{max} as:

$$\varepsilon = \sqrt{1 - 1/S_g} \frac{\sin \delta_{max}}{\left(2 \frac{I_y}{I_x} - 1 \right)} \quad (2.31)$$

This leads to the values of ξ_0 and ξ'_0 necessary to compute the epicycle trajectory. Note that it is not necessarily true that the real fired projectile, for which we measured δ_{max} , had a non-zero value of in-bore yaw. That is because the cause δ_{max} could be both in-bore yaw and dynamic unbalance. The measured effect is virtually the same (that is why both are referred by the same symbol ε), but distinguishing which of the two causes is the right one is often not easy during tests.

The previous analytic process is explained in the article "Influence of chamber misalignment on cased telescoped (CT) ammunition accuracy"[2] by D. Corriveau and C. Florin Petre from the Defense R&D department of Canada. In this article they also studied the experimental correlation between chamber misalignment and first maximum yaw δ_{max} , validating the analytic model.

2.4 Lateral Deflection

It is now interesting to delve into the concept of lateral deflection connected to projectile gyroscopic motion. As seen in section 2.3, the projectile is considered to generally have both static and dynamic unbalance, due to the in-bore yaw that retains while travelling down the barrel, and ultimately exiting at the muzzle. When the projectile exits from the barrel, the constraints imposed on its motion are abruptly removed. Due to the unbalances, a deflection from the nominal path quickly develops. This deflection has three major components, which arise from distinct principles: **Aerodynamic Jump**, **Lateral Throw-off** and **Gyroscopic Drift**. The first in-depth study of this deflection was made by F. W. Mann in "The Bullet's Flight from Powder to Target"[3], which referred to the Lateral Throw-off as "X-Error" and the Aerodynamic Jump as "Y-Error". He was also the first to discover that this two effects can be arbitrarily obtained by drilling holes in bullets.

2.4.1 Aerodynamic Jump

The Aerodynamic Jump, J_A , is caused by the dynamic unbalance angle ε , which in our case, as previously explained, is exactly the in-bore yaw, and therefore the first yaw angle that the projectile has during its trajectory.

Immediately after exiting the muzzle, the projectile moves forward while simultaneously being tilted of an angle ε . From the body reference frame of the projectile, this condition is equivalent of having $\varepsilon = 0$ and a relative wind component, of magnitude $w = V_0 \sin \varepsilon$, directed from the barrel axis to the tip of the projectile. This is the exact same situation of a rotating cylinder invested by a uniform fluid current. For the Magnus effect, the rotation of the projectile causes air to be faster on one side, resulting in a transversal pressure gradient that develops a force, called the Magnus Force. This force is the cause for the Aerodynamic Jump effect.

For an upward-pointing projectile ($\varepsilon > 0$ and $\varphi_0 = 0$) with a right-hand twist, the lateral deflection due to the Aerodynamic Jump is on the left, from the shooter perspective.

The value J_A is defined as the tangent of the angle between the barrel and the component of the deflected flight due to the Aerodynamic Jump. It's possible to derive the analytic relation between J_A and ε , obtaining the expression:

$$J_A = -i \left[\left(\frac{2\pi}{n} \right) (k_y^2 - k_x^2) \left(\frac{C_{L\alpha}}{C_{M\alpha}} \right) \sin \varepsilon \right] e^{i\varphi_0} \quad (2.32)$$

where n is the rifling twist rate in calibers/turn. k_y^2 and k_x^2 are respectively $I_y/(md^2)$ and $I_x/(md^2)$.

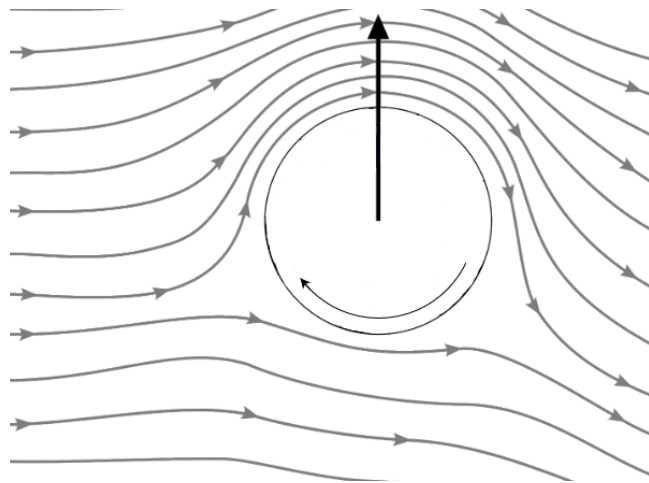


Figure 2.3: Magnus effect schematization. A clockwise rotating cylinder immersed in a left-to-right flow experiences a vertical force that points up. This effect is the cause of the Aerodynamic Jump component of deflection.

2.4.2 Lateral Throw-off

The Lateral Throw-off effect is caused by the static unbalance $\hat{\varepsilon}$. when the projectile travels in the barrel it is constrained to the motion imposed by the rifling. If it enters with a tilt, the center of mass traces a helical path along the barrel, which is a circumference of radius $\hat{\varepsilon}$ if we look at it from behind. When the projectile exits from the muzzle, the center of mass, in addition to the forward velocity, has a lateral velocity component tangent to the final point of the circular path. The projectile essentially tends to fling off as soon as it leaves the barrel.

As for the definition of J_A , also the Lateral Throw-off T_L is defines as the tangent of the angle between the barrel and the component of the deflected flight due to it. The analytic

expression that relates the in-bore yaw ε to T_L is:

$$T_L = i \left[\left(\frac{2\pi}{n} \right) \left(L_N + \frac{1}{2} L_{CYL} - XCG \right) \sin \varepsilon \right] e^{i\varphi_0} \quad (2.33)$$

where n is the rifling twist rate in calibers/turn, L_N is the length of the ogive section of the projectile, L_{CYL} is the length of the cylindrical center section of the projectile and XCG is the distance of the center of gravity from the tip.

Note that the term that contains the geometric quantities L_N , L_{CYL} and XCG is positive if the XCG is in front of the mid-point of the cylindrical section. This is in agreement with the fact that the Lateral Throw-off, for an upward-pointing projectile ($\varepsilon > 0$ and $\varphi_0 = 0$) with a right-hand twist, is on the right.

2.4.3 Gyroscopic Drift

The Gyroscopic Drift effect is caused by the presence of the yaw of repose β_R . The cause of the development of a yaw of repose due to the gyroscopic behaviour of the projectile has been already explained in section 2.1. Due to this persistent yaw in flight, a lateral force continuously acts on the projectile, making the Gyroscopic Drift approximately proportional to the square of the distance travelled. For right-hand spinning projectiles the drift is to the right, from the shooter perspective. For short distances, however, this component of the lateral deflection is negligible with respect to the Aerodynamic Jump.

The analytical expression that relates the dimensionless distance s to the Gyroscopic Drift, in calibers, is:

$$D_R \approx ik_y^2 \left(\frac{PG_0}{2} \right) \left(\frac{C_{L_\alpha}}{C_{M_\alpha}} \right) s^2 \left[1 + \frac{2}{3} (C_D^* s) + \frac{1}{3} (C_D^* s)^2 \right] \quad (2.34)$$

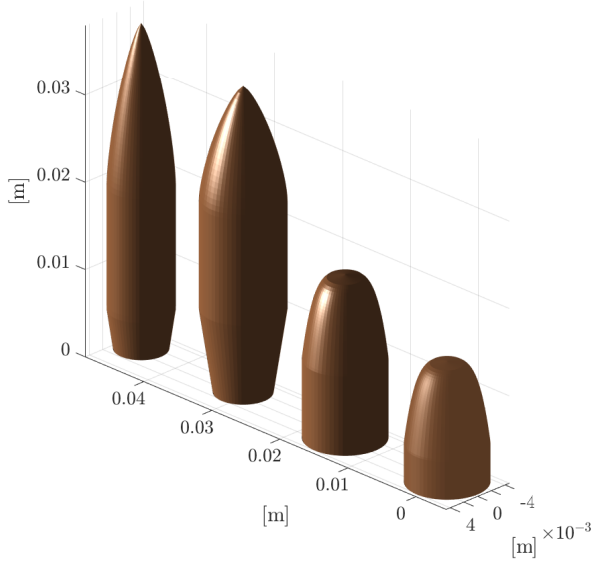
This equation is not adequate for long distances ($\gtrsim 1000$ m), and a better approach is to use computations based on the point-mass model or 6-DOFs model.

Chapter 3

bulletStability Code

A MATLAB® code, called `bulletStability`, was written specifically for this report. The code is able to compute the epicycle trajectory of a projectile, given its geometry and aerodynamic coefficients. If the aerodynamic coefficients provided depend on Mach number, the code also takes it into account, making the projectile slow down during flight (following Equation 1.18). It's also possible to turn "on" or "off" the damping in roll computation, that causes the spin of the projectile to slow down. Along with all the quantities relative to the epicycle trajectory, it also computes the lateral deflection components explained in section 2.4. Finally, a 3D animation of the projectile motion was developed to better visualize it. The entire repository of the code is publically available on GitHub. The animated gyroscopic motions for the trajectories studied in this chapter have been assembled in this video. In the present analysis, every bullet is supposed to have a maximum first yaw δ_{max} of 5° . This is a simplification due to the fact that each weapon-bullet pair will have an experimentally found average δ_{max} . The 5° value is a mean value for military rifle projectiles tested in "The initial yaw of some commonly encountered military rifle bullets"[4] article by Peter Knudsen. The effect of different δ_{max} on the epicycle trajectory is approximately the same as of a scaling factor, therefore every considerations about the general gyroscopic behaviour of the bullets are still valid.

3.1 Governing Equations and Code Diagram



Every equation used in the code has already been reported and appropriately commented on in previous chapters of this report. For ease of visualization, all equations used are reported in Appendix B. The steps performed by the code to calculate the epicycle trajectory are illustrated in the block diagram Figure 3.1. Using the code, we are now gonna analize the stability behaviour of the following bullets:

- 9x19mm Parabellum 124gr
- 9x19mm Parabellum 158gr
- 9x39mm SP-5
- Twenty-nine 7mm bullet for hunting

All analysis were conducted at an atmospheric temperature of $T = 298K$ ($\approx 25^\circ C$), air density $\rho = 1.225kg/m^3$ and a standard gravitational acceleration of $9.81m/s^2$.

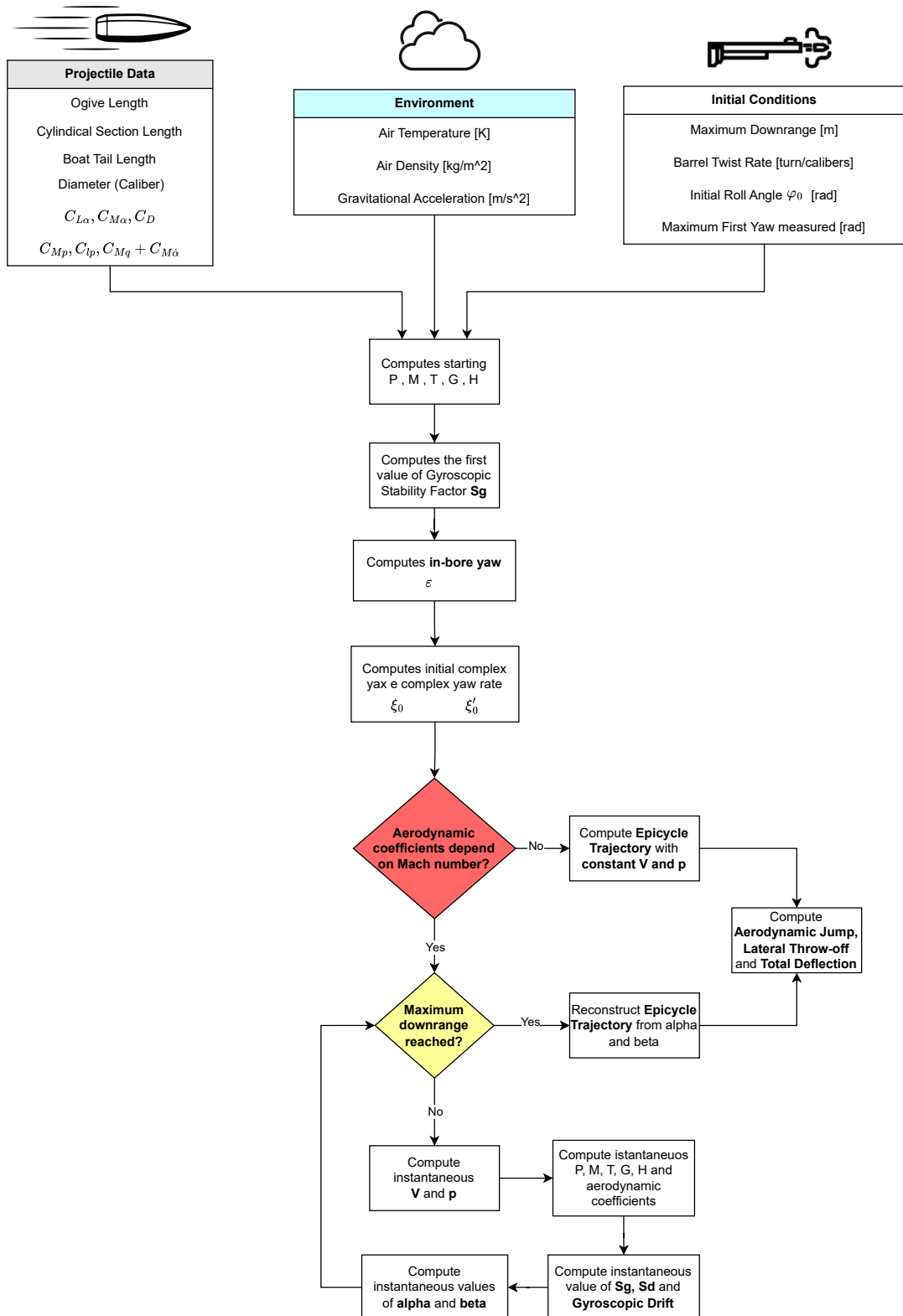


Figure 3.1: Block diagram that schematize the bulletStability code

3.2 9x19mm Parabellum

The 9x19mm Parabellum, also known as 9mm Luger, is one of the most widely used bullets, both in dynamic shooting competitions and by the police. We consider two 9x19mm Parabellum FMJ bullets (one of 124 and one of 158 grains) to be fired from a Beretta 92 FS, which usually has a rifling twist rate of 1:9.84 turn/inches. The bullets geometry are shown in Figure 3.2 and Figure 3.3. The initial conditions and results are tabulated in Table C.1 and Table C.2.

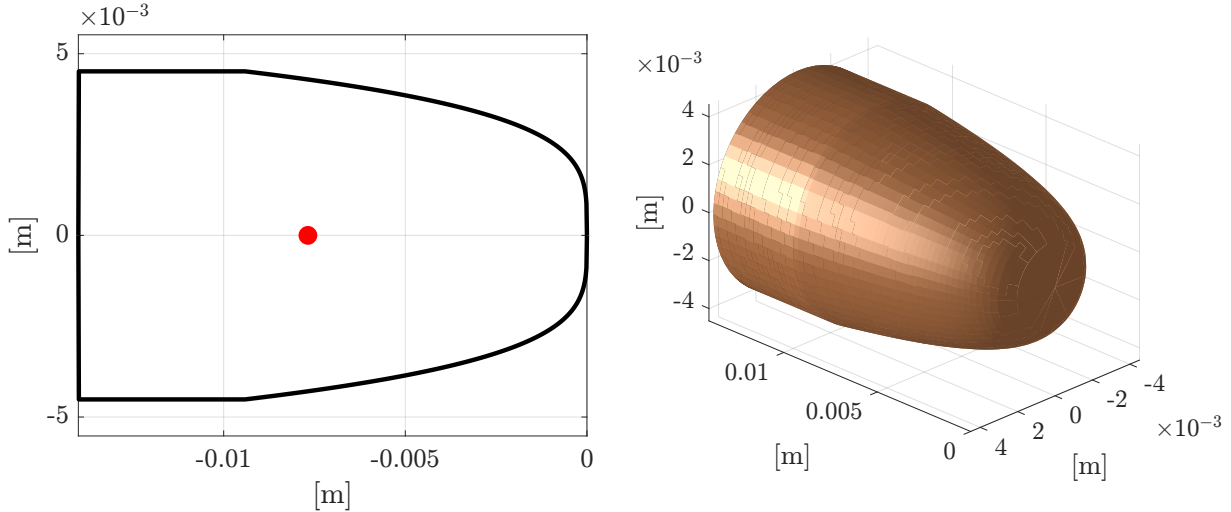


Figure 3.2: 9x19mm Parabellum 124 grains geometry

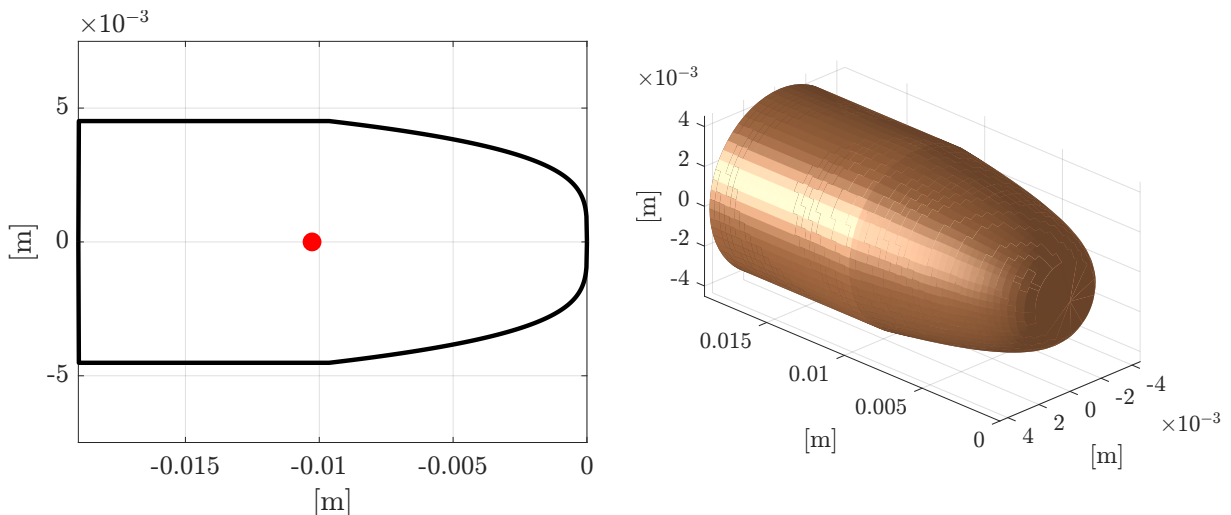


Figure 3.3: 9x19mm Parabellum 158 grains geometry

Figure 3.4 and Figure 3.5 show the epicycle trajectory of the two bullets during flight. The first thing that can be stated is that the overall gyroscopic behaviour is of the same nature: for both bullets the arms of precession and nutation are comparable, but nutation is an order of magnitude faster than precession. More precisely for the 124gr one, nutation has a frequency that spans from 471Hz to 417Hz, while precession spans from 13Hz to 9.6Hz. The 158gr bullet has the same frequencies for precession, but considerably slower frequencies for nutation, due to its higher inertia, spanning from 270Hz to 255Hz.

This slower precession frequency of the 158gr has a considerable effect on the angle α_{tot} that the bullet will have once it meets the target, since it needs to travel a greater distance to experience the same decrease in α_{tot} . This effect can be seen in Figure 3.6 and Figure 3.7. The

124gr reaches the 100m mark with $\alpha_{tot} = 0.55^\circ$, while the 158gr with $\alpha_{tot} = 1.19^\circ$. This angle has to be taken into account for terminal ballistic consideration, since generally the damage caused to soft targets is directly related to it.

Another important aspect is that, due to its lower initial velocity, the 158gr bullet enters the subsonic regime (considered to be at $Ma < 0.85$) at a shorter distance in comparison to the 124gr one. Note, however, that even if both bullets technically start their flight in transonic regime, the 124gr one exit the muzzle at $Ma = 1.04$, which is already in a range where shockwaves begin to form in front of the bullet. These shock waves are a problem acoustically, as they add up to the sound of the shoot. The 158gr, on the other hand, exits at $Ma = 0.92$, avoiding this problem. Shooting with 158gr bullets results in a quieter shooting experience. The evolution of Mach number during flight can be seen in Figure 3.8, along with the evolution of the C_D and $C_{L\alpha}$ coefficients, which are closely related to dynamic stability.

Finally, it is possible to observe the effect of the higher ballistic coefficient of the 158gr bullet on the final velocity: even if the 124gr bullet exits the muzzle 42m/s faster than the 158gr one, at 100m they have a difference of merely 4m/s.

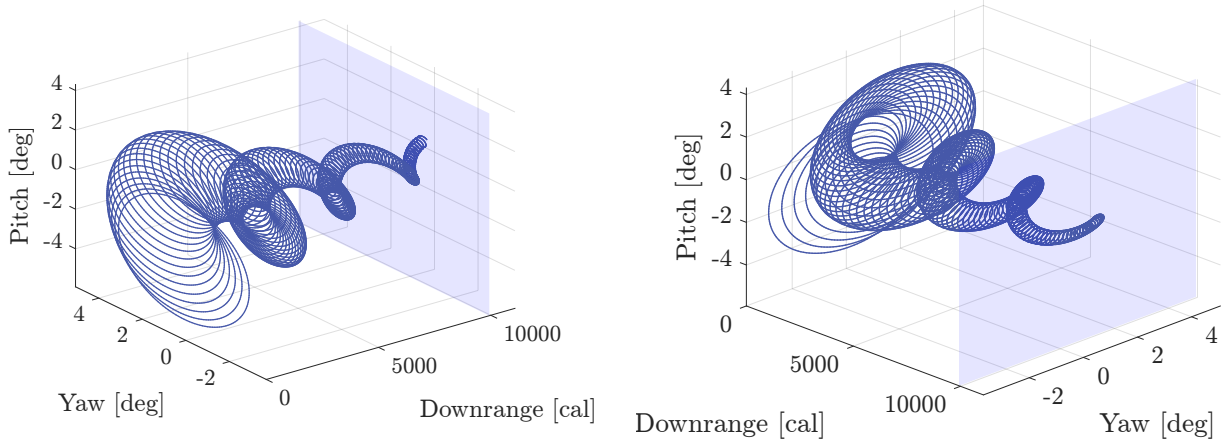


Figure 3.4: 3D epicycle trajectory of 9x19mm Parabellum 124gr. The blue plane identifies the transition from transonic to subsonic regime.

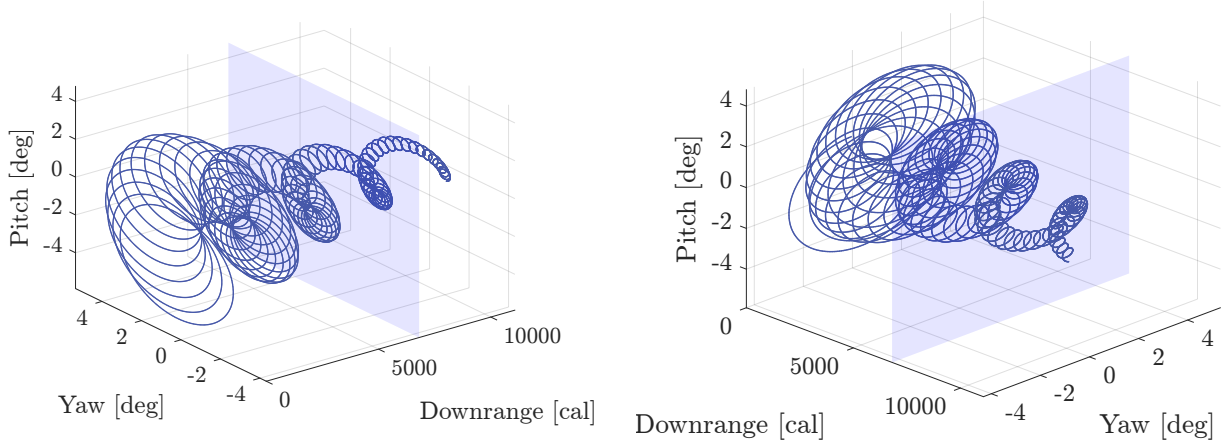


Figure 3.5: 3D epicycle trajectory of 9x19mm Parabellum 158gr. The blue plane identifies the transition from transonic to subsonic regime.

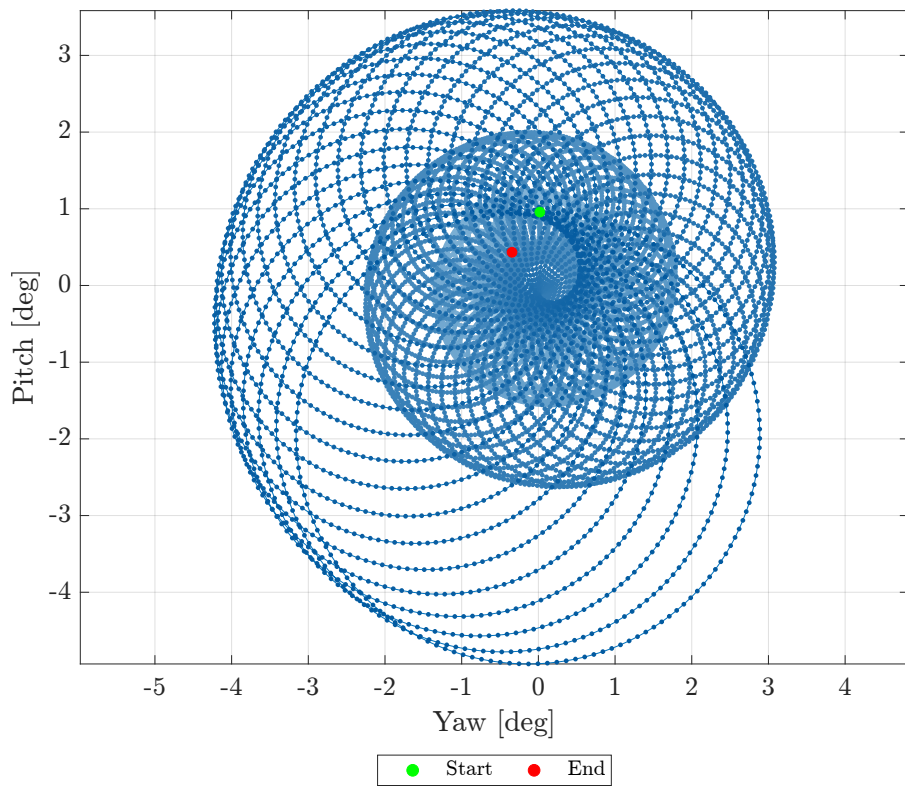


Figure 3.6: 9x19mm Parabellum 124gr epicycle trajectory from the muzzle perspective

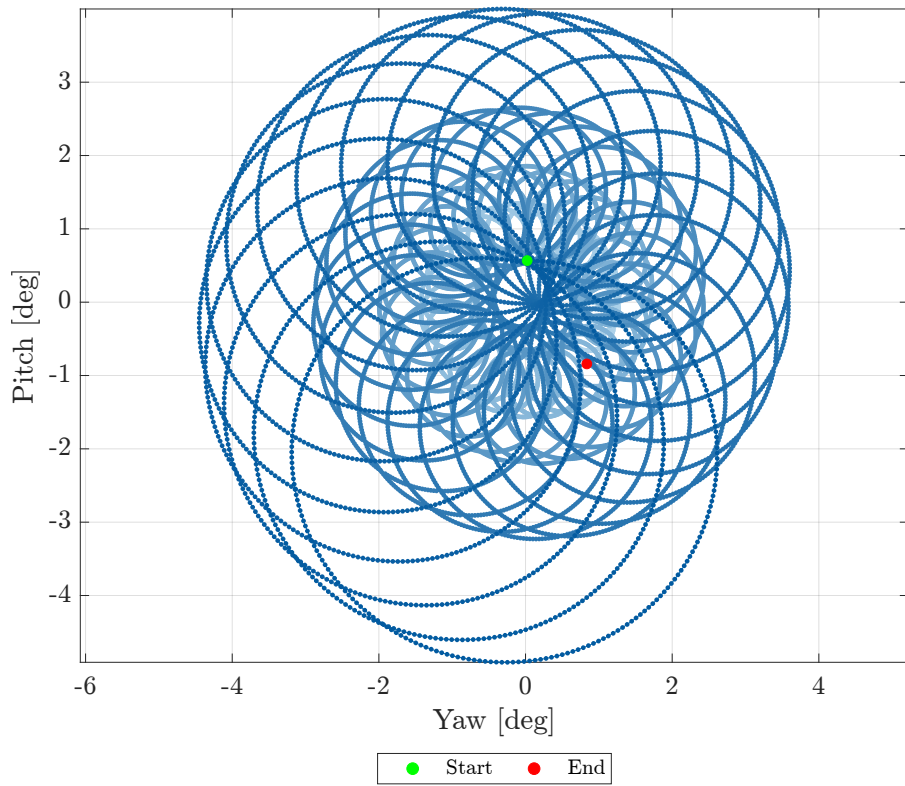


Figure 3.7: 9x19mm Parabellum 158gr epicycle trajectory from the muzzle perspective

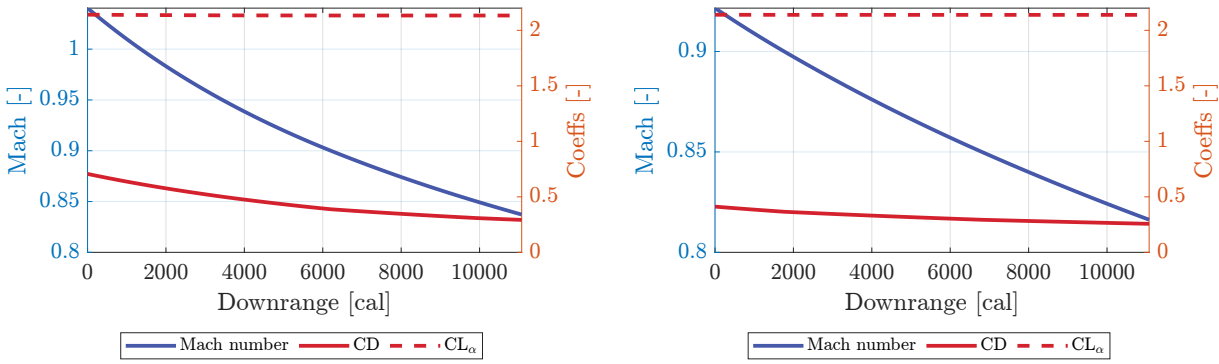


Figure 3.8: Mach number, aerodynamic drag coefficient and lift coefficient derivative during flight of 9x19 Parabellum 124gr and 158gr respectively

Regarding gyroscopic and dynamic stability, Figure 3.9 shows the behaviour of the two bullets in the classic S_g vs S_d plane. Two important things can be noticed:

1. The 124gr has a greater excursion of S_g . This is always due to the fact that the 124gr has a lower ballistic coefficient than the 158gr. The 124gr velocity V drops faster than the 158gr one, but they have no significant difference in the damping in roll.
2. Both bullets are gyroscopically over-stabilized. The consequence is that they will be less accurate than if they were fired with an appropriate S_g . The reason of having this amount of gyroscopic stability could lay in the fact that these bullets are not designed to hit targets further than 100m, and in this range the deflection due to spin rate is marginal. As seen, the faster a bullet spins, the faster its α_{tot} decreases. Therefore the reason for this over-stabilization could lay in the terminal ballistic characteristics of them. Problems of tractability of the trajectory could occur for this high amount of gyroscopic stability, but since these bullets are designed to have a short effective range, this problem is relatively contained.

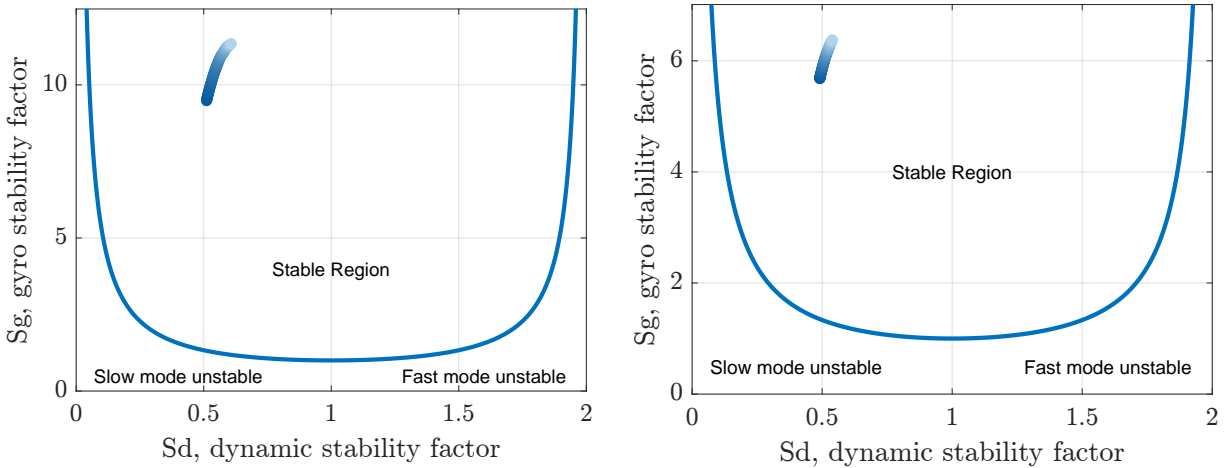


Figure 3.9: Stability diagram for 9x19 Parabellum bullets weighting 124gr and 158gr. The evolution of the point in the diagram goes from the darkest to the lightest color.

The Gyroscopic Drift deflection component and the deflection due to Aerodynamic Jump and Lateral Throwoff are shown in Figure 3.10 for the 124gr and Figure 3.11 for the 158gr. Since it weighs less, the 124gr bullet spins faster, resulting in a major lateral deflection both in terms of Gyroscopic Drift and Aerodynamic Jump.

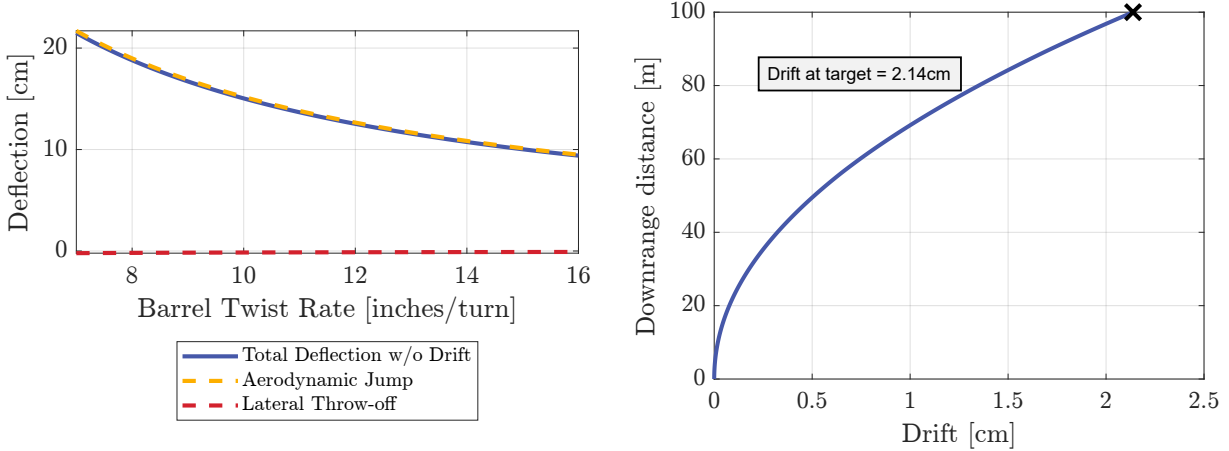


Figure 3.10: 9x19mm Parabellum 124gr deflection components: Aerodynamic Jump and Lateral Throw-off deflection with respect of rifling twist rate. On the right Gyroscopic Drift vs Downrange.

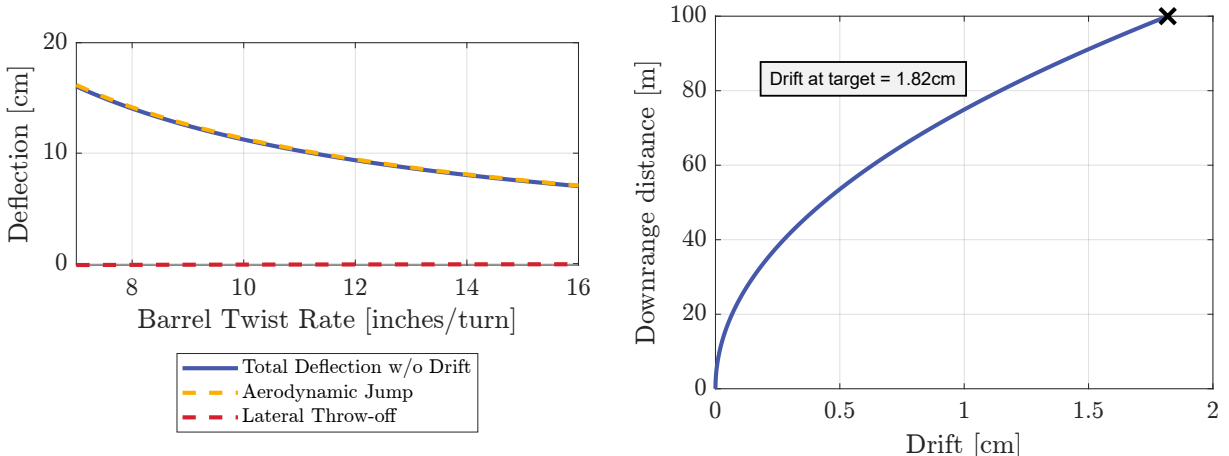


Figure 3.11: 9x19mm Parabellum 124gr deflection components: Aerodynamic Jump and Lateral Throw-off deflection with respect of rifling twist rate. On the right Gyroscopic Drift vs Downrange.

3.3 9x39mm SP-5 Subsonic Bullet

The 9x39mm is a caliber popular in Post-Soviet states that was developed in the '80s by Russia with the objective of manufacturing a subsonic stealthier bullet capable of penetrating personal body armor at distances up to 400m. In these report we will analyse the SP-5 version, which is the first massively produced version of this caliber. Its purpose requires it to have a higher inertia than standard 9mm bullets, which is achieved by weighting it at 16.1g. We consider it fired from a VSS "Vintorez" sniper rifle, which is one of the most common weapon that shoots this caliber. The VSS has a rifling twist rate of 1:8.3 turn/inches. All the results can be found in Table C.3.

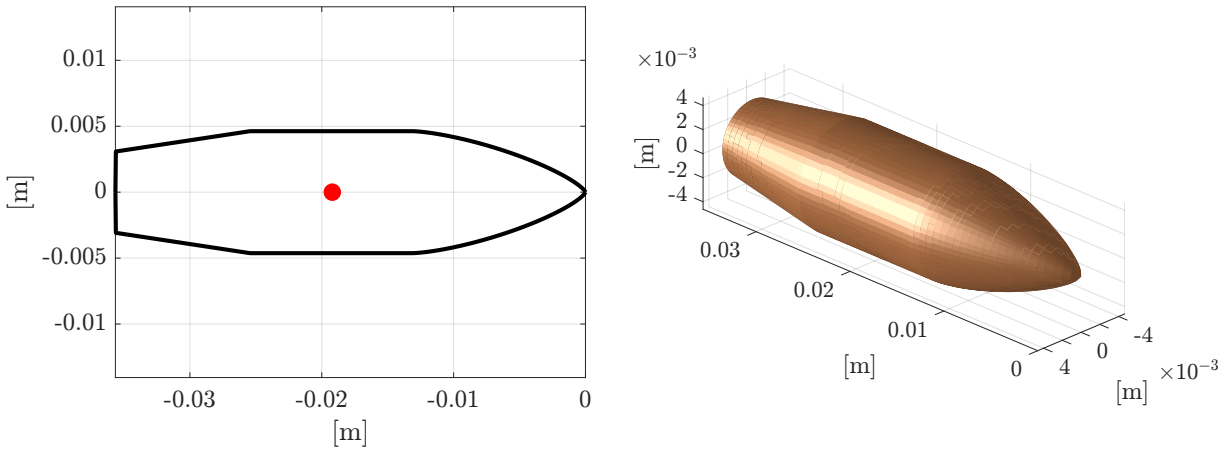


Figure 3.12: 9x39mm SP-5 geometry

The gyroscopic behaviour of the bullet is visualized in Figure 3.13 and Figure 3.14. Unlike the 9x19mm, the 9x39mm precession and nutation have similar arm lengths at the start, but the latter decreases quickly, leaving basically only a precession movement across the whole 400m flight. The precession frequency spans from 17.6Hz to 13.9Hz, while the nutation frequency spans from 130Hz to 116Hz. Since nutation is quickly damped out, its frequency has no significance after a short distance. On the other hand, precession does not experience much damping, leaving the projectile precess with almost the same α_{tot} during the whole flight.

The 1:8.3 turn/inches rifling twist rate gives marginal stability to the bullet (as seen in Figure 3.16), indicating that the designed process focussed on accuracy. A faster rifling rate will dump out even the precession movement, at the possible expense of accuracy. It is curious to notice how the point in the stability graph "climbs up" and enters the stable region even if it starts in an unstable region. This behaviour is not strange and it is expected for the reason explained in subsection 1.3.1, the spin rate decreases at a slower rate than the linear velocity does. If the C_{l_p} of the projectile had been higher, there was a possibility that the precession would have become unstable, as is the case in the test shown in Figure 3.17. This is also an example of how classic gyroscopic stability does not imply dynamic stability.

Similarly to the 158gr 9x19mm Parabellum, The 9x39mm SP-5 exits the muzzle at transonic regime but a speed for which shockwaves do not form, decreasing the noise made by the shot. The Mach number, C_D and $C_{L_{a\alpha}}$ during flight are shown in Figure 3.15, while the deflection components are shown in Figure 3.18.

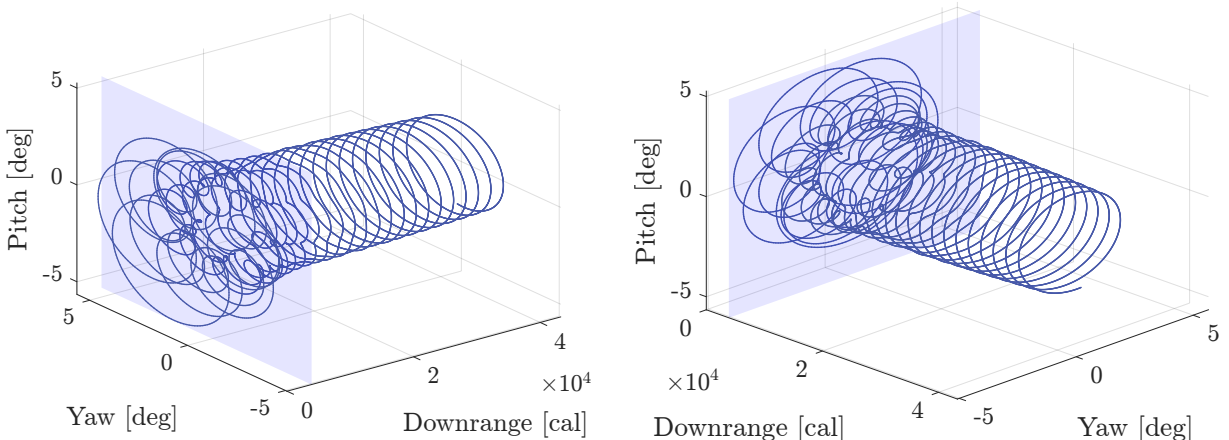


Figure 3.13: 3D epicycle trajectory of 9x39mm SP-5. The blue plane identifies the transition from transonic to subsonic regime.

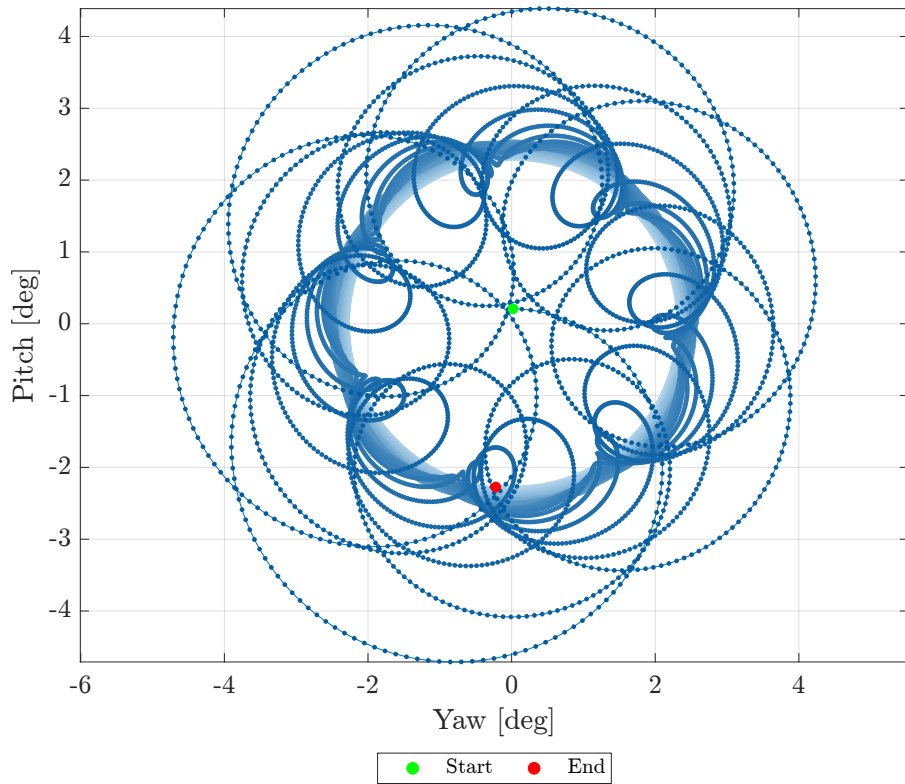


Figure 3.14: 9x39mm SP-5 epicycle trajectory from the muzzle perspective.

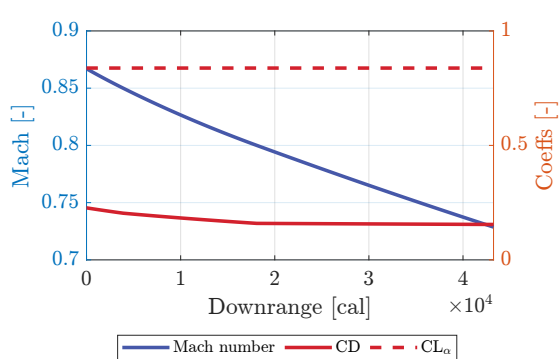


Figure 3.15: Mach number, aerodynamic drag coefficient and lift coefficient derivative during flight of 9x39mm SP-5.

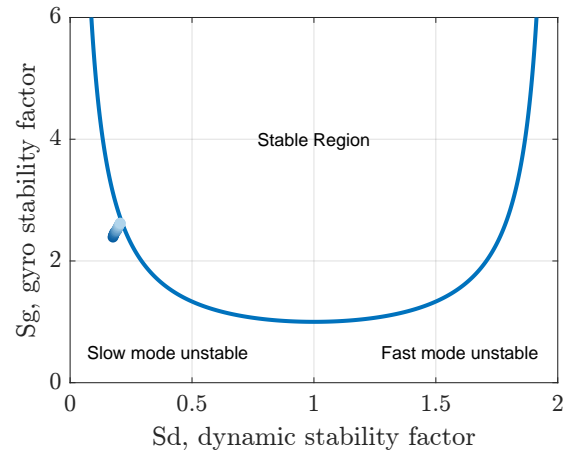


Figure 3.16: Stability diagram for 9x39mm SP-5. The evolution of the point in the diagram goes from the darkest to the lightest color.

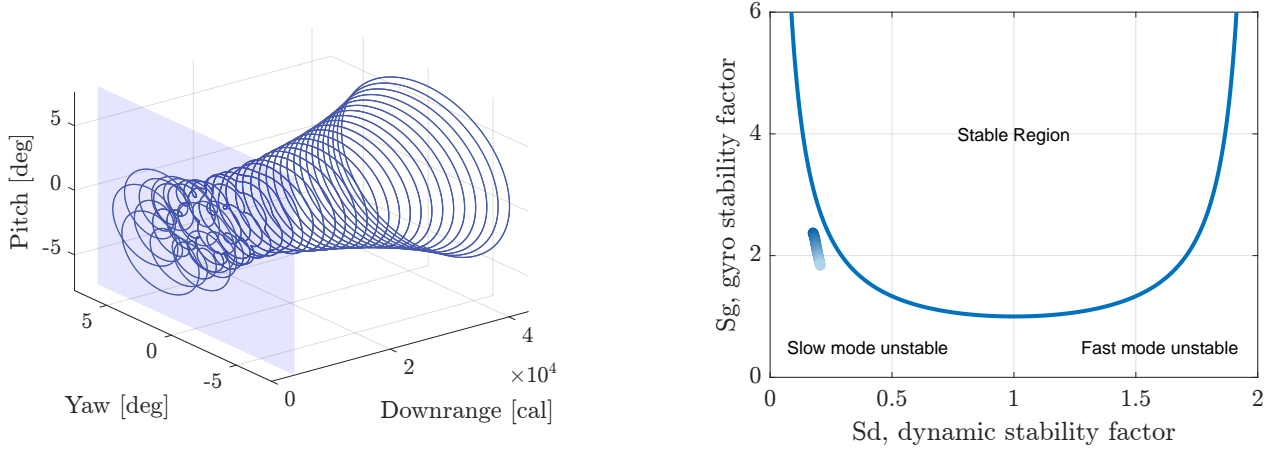


Figure 3.17: Epicycle trajectory and stability diagram for a 9x39mm with higher damping in roll. The evolution of the point in the diagram goes from the darkest to the lightest color.

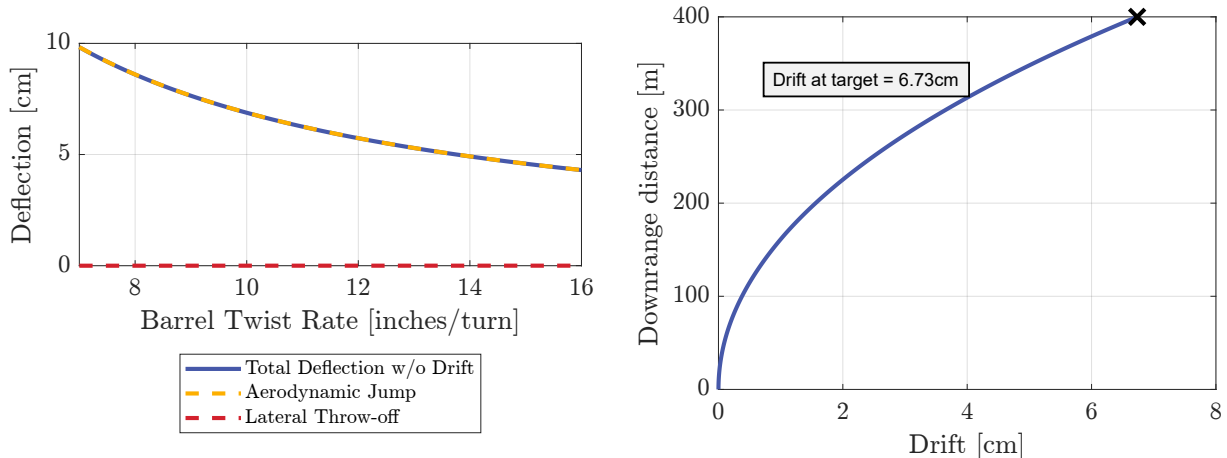


Figure 3.18: 9x39mm SP-5 deflection components: Aerodynamic Jump and Lateral Throw-off deflection with respect of rifling twist rate. On the right Gyroscopic Drift vs Downrange.

3.4 7mm Bullet

This 7mm bullet is designed for hunting mid-to-big size animals and is supposed to fly at an high supersonic regime. It weights 10g (154.3gr) and can be shot from a variety of rifling twist rate, here it was selected a 1:7.3 turn/inches one. All the main results can be found in Table C.4. The bullet exits the muzzle at $Ma = 2.45$, reaching a downrange of 300m at $Ma = 2.02$. The Mach number during flight can be seen in Figure 3.22.

The epicycle trajectory (Figure 3.20 and Figure 3.21) along with the stability diagram (Figure 3.23) show that nutation damps out almost immediately, while precession starts off a bit unstable but after approximately 150m it becomes stable and its arm starts to decrease.

Figure 3.24 shows how, even though this bullet rotates almost 10 times faster than all the others analysed, it is the one that drifts the least. This is due to the fact that the Gyroscopic Drift does not depend solely on the spin rate, but it depends on the p/V ratio.

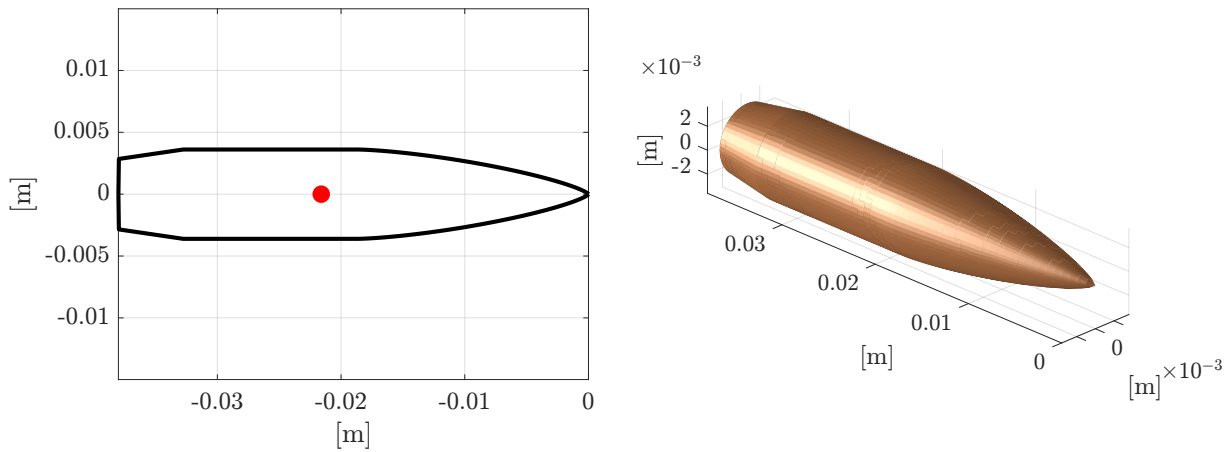


Figure 3.19: 7mm hunting bullet geometry

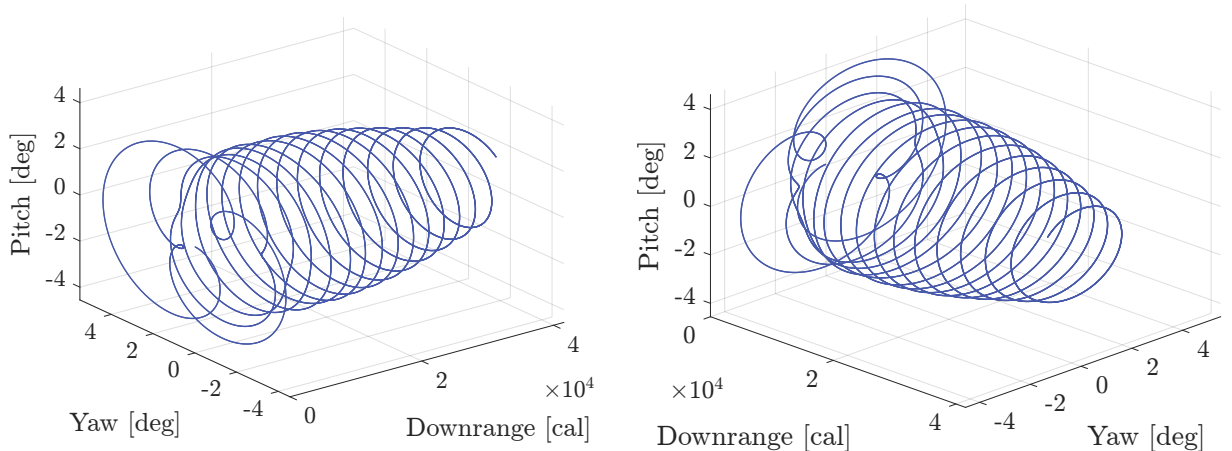


Figure 3.20: 3D epicycle trajectory of 7mm bullet.

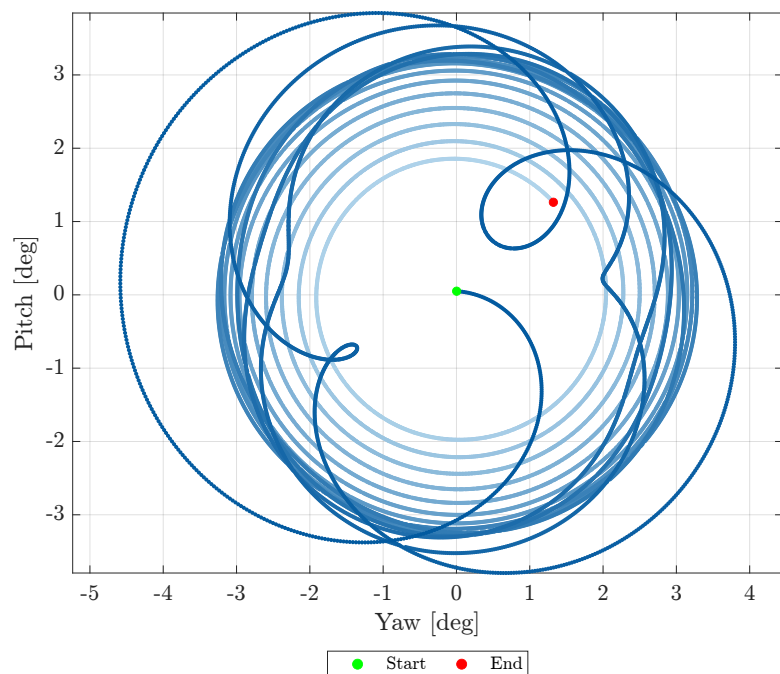


Figure 3.21: 7mm epicycle trajectory from the muzzle perspective

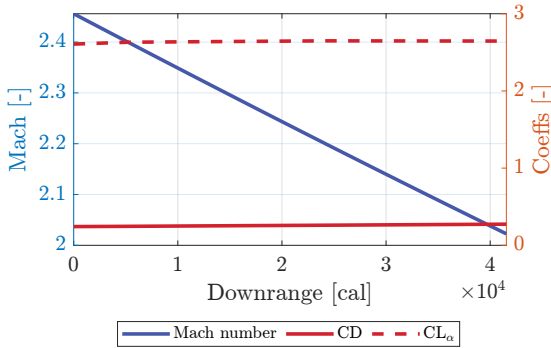


Figure 3.22: Mach number, aerodynamic drag coefficient and lift coefficient derivative during flight of the 7mm bullet.

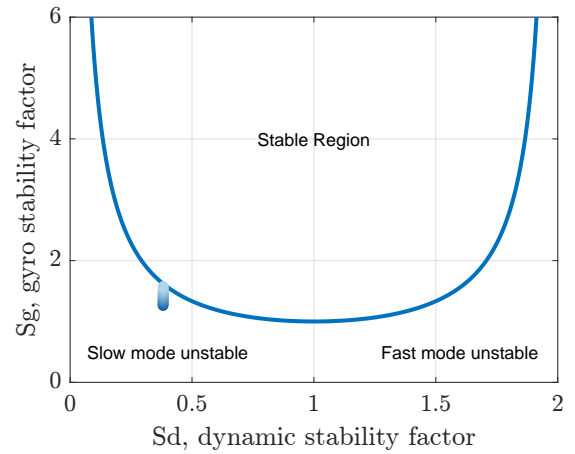


Figure 3.23: Stability diagram for the 7mm bullet. The evolution of the point in the diagram goes from the darkest to the lightest color.

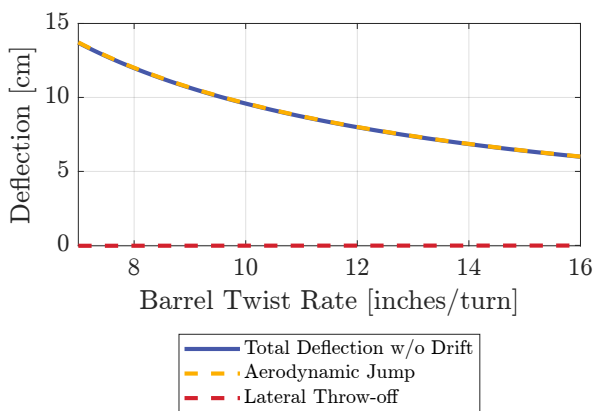


Figure 3.24: 7mm bullet deflection components: Aerodynamic Jump and Lateral Throw-off deflection with respect of rifling twist rate. On the right Gyroscopic Drift vs Downrange.

It is of interest now to look at the effect of rifling twist rate on this 7mm bullet. The effect can be seen in Figure 3.25: The first thing that can be noticed is that the nutation frequency increases with an increase in rifling twist rate (the 1:5 rifling has the fastest nutation frequency). It does not only affect frequency but also damping. The slower the rifling rate the higher the damping on nutation.

The rifling, on the other hand, does not affect the precession frequency as much as for nutation. The primary effect is in the damping: from 1:5 to 1:8.2, the α_{tot} caused by precession is significantly different, increasing at the point that for rifling twist slightly slower than 1:8.2 the projectile is dynamically unstable. It is also important to state that the "Linear Theory for Spin-Stabilized Projectiles" is only valid up to $\alpha_{tot} \approx 15^\circ$, therefore, even if the code shows no dynamic instability, a check on the value reached by α_{tot} is always needed. Figure 3.26 shows all the trajectories of Figure 3.25 in a single plot for a better comparison.

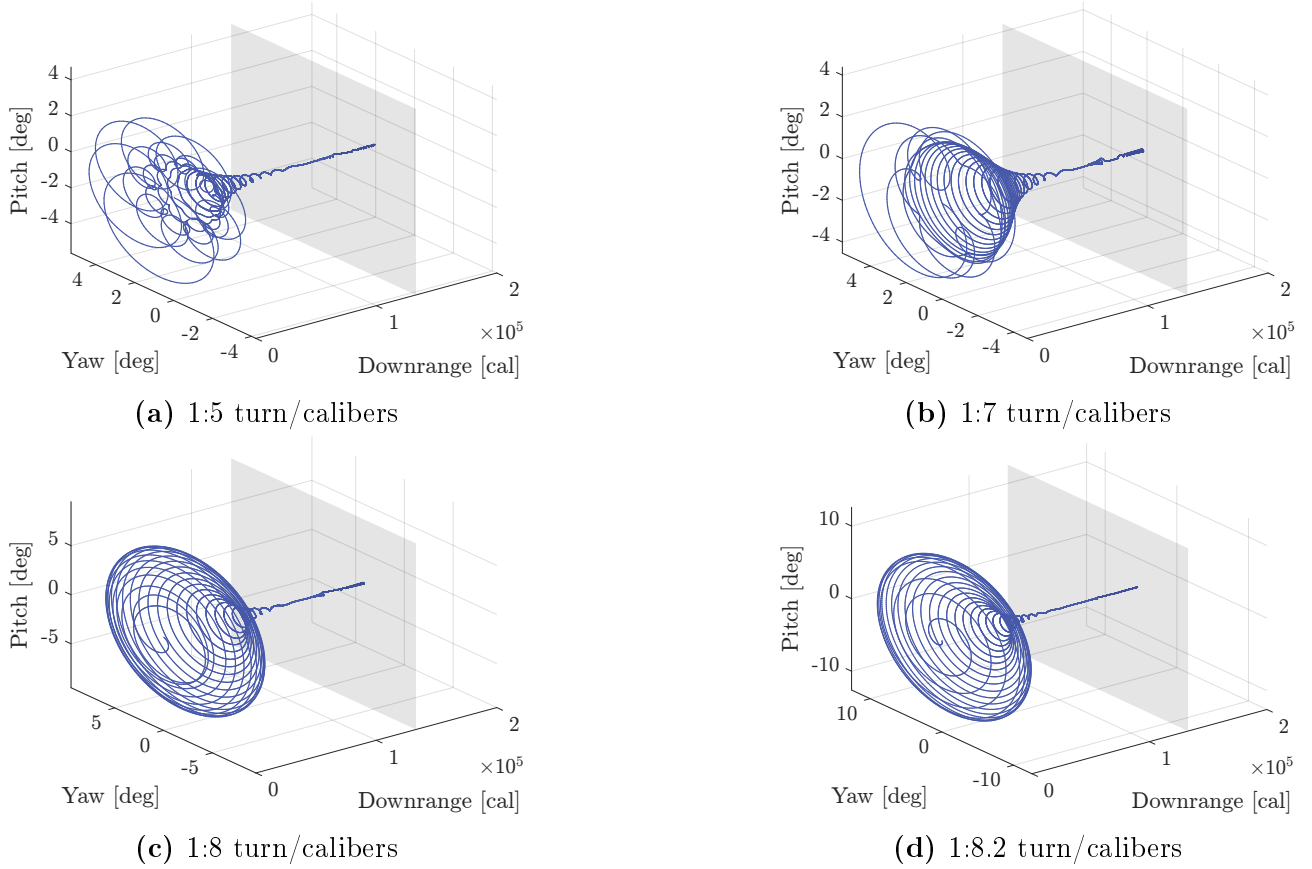


Figure 3.25: 7mm bullet fired from different rifling twist rate. The grey plane represents the downrange value for which the bullet enters the transonic regime, which in this case is of $\approx 960m$.

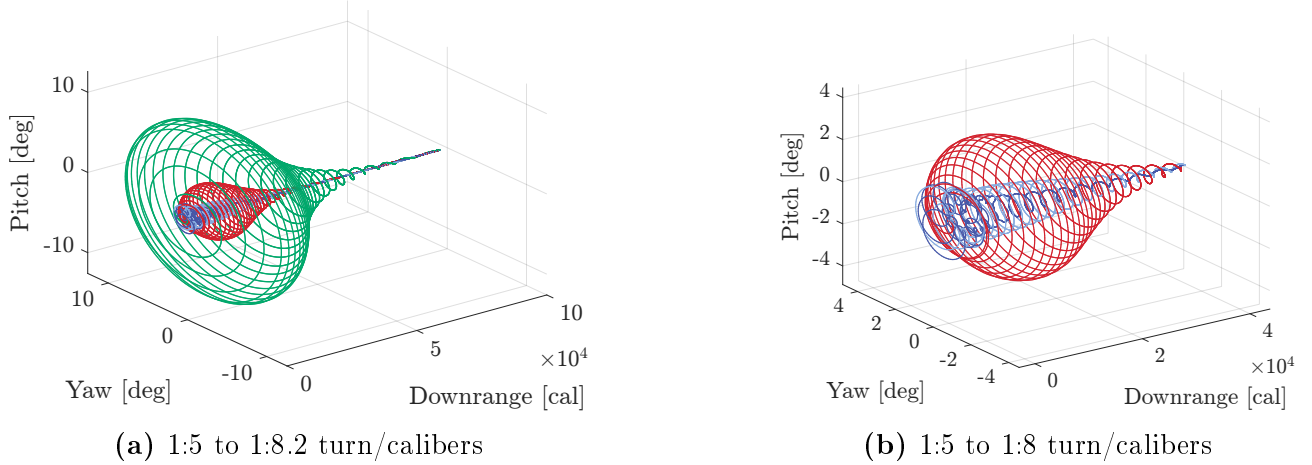


Figure 3.26: (a) showing all the previous trajectories of the 7mm shot by different riflings. Figure (b) is a detail of Figure (a).

Finally, Figure 3.27 shows a detail of the epicycle trajectory of the 7mm fired from a 1:7 turn/calibers rifling, enfiting the phase of the flight where the bullet is in the transonic regime. In this regime most of the aerodynamic coefficients change due to the shifting in the position of the shockwaves on and around the bullet. The coefficients that are mostly affected by this phenomena are the C_D and the $C_{L\alpha}$, closely related to gyroscopic and dynamic flight stability. The general result is that all bullets tend to lose stability in this section, and while the 7mm in

question is not very affected by it, this phenomena needs to be taken into account during the design process.

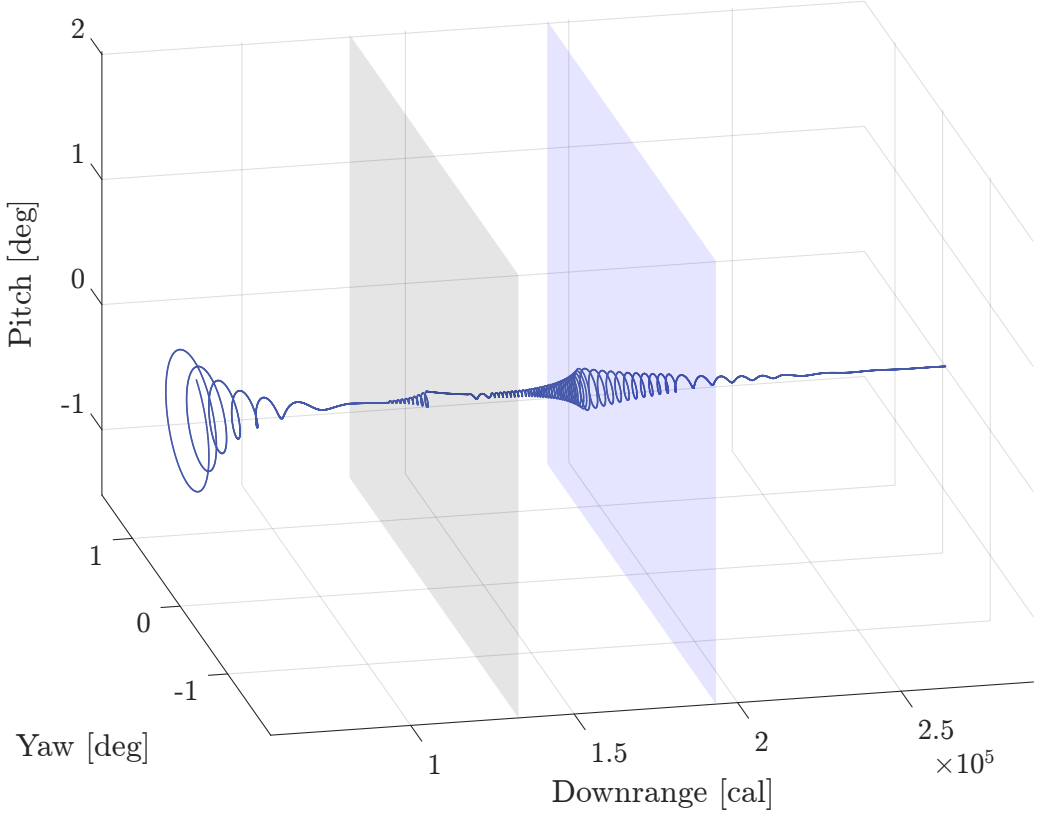


Figure 3.27: 7mm epicycle trajectory from the muzzle perspective

3.5 Comparison with Miller's Formula

Miller's formula is a widely used formula useful for the computation of the rifling twist rate needed to achieve optimal gyroscopic stability. This formula is very convenient because it directly relates the bullet geometry with the gyroscopic stability factor and the rifling twist rate. The formula is here presented:

$$n^2 = \frac{30m_{gr}}{S_g d_{inch}^3 l_{cal} (1 + l_{cal}^2)} \quad (3.1)$$

where m_{gr} is the bullet mass in grains, S_g is the gyroscopic stability factor, d_{inch} is the bullet diameter in inches, l_{cal} is the bullet length in calibers and n is the twist rate in calibers/turn.

The value that is usually recommended for S_g is 2, therefore the comparisons have been done with this value for the gyroscopic stability factor.

Table 3.1 shows the twist rate resulting from Miller's formula for the previously studied bullets. The value of the twist rate for the Linearized Theory is instead the slowest possible twist rate for which the bullets are considered stable (i.e. the maximum α_{tot} does not exceed 15°). This comparison is useful to see if Miller's formula gives as output values of twist rate for which the Linearized Theory computes dynamic instability.

The results show how Miller's Formula gives a value of rifling for which we have instability for every bullet except for the 7mm one. This is probably due to the fact that the term $l_{cal}(1 + l_{cal}^2)$ comes from the assumptions made for the shape of the projectile. Miller's formula, in the shape reported here, is better suited for slender bullets like the 7mm than for blunt bullets like the

9x19mm. Matter of fact, Miller's formula works really well for the 7mm, indicating an optimal twist rate of 7.34, which is almost exactly the value studied to be well suited for this bullet in section 3.4.

Table 3.1: Comparison between the twist rate, in calibers/turn, resulting from Miller's formula and the twist rate needed for marginal stability resulting from the Linearized Theory

Bullet	Miller's formula	Linearized Theory
9x19mm 124 grains	31.4	30.2
9x19mm 158 grains	24.2	23.4
9x39mm SP-5	12.9	11.2
7mm	7.34	8.2

Chapter 4

Conclusions

In conclusion, the "Linearized Theory of Spin-Stabilized Bullets" provides effective methods to study the gyroscopic behaviour of projectiles through closed analytical solutions. By applying this theory it was possible to write the `bulletStability` code, thanks to which we investigated projectiles gyroscopic motions at a computational cost that was far lower than that of more intricate 6 Degrees of Freedom models.

In addition, it was possible to identify and quantify the various factors affecting gyroscopic stability and lateral deflection, offering concrete insights for improving both external and terminal ballistic performance of projectiles.

Finally, comparison of Miller's formula with simulation highlighted the range of validity of the formula for projectile stability analysis, showing how both can be useful tools in the ballistic design process.

To summarize, this research validates the value of the Linearized Theory as a significant tool for munitions design. It is particularly helpful in providing direct and understandable insights into the flight dynamics of projectiles, in addition to its computing efficiency.

Bibliography

- [1] R. McCoy. *Modern Exterior Ballistics: The Launch and Flight Dynamics of Symmetric Projectiles*. A Schiffer design book. Schiffer Publishing, 1999.
- [2] D. Corriveau and C. Florin Petre. Influence of chamber misalignment on cased telescoped (ct) ammunition accuracy. *Defence Technology*, 12(2):117–123, 2016. 2016 International Symposium on Ballistics.
- [3] Franklin W Mann. *The Bullet’s Flight from Powder to Target*. Ravenio Books, 1909.
- [4] Peter Knudsen and Ole Sørensen. The initial yaw of some commonly encountered military rifle bullets. *International journal of legal medicine*, 107:141–6, 02 1994.

Appendix A

Derivation Process for the Equations of Motion

We re-state the general Equations of Motion in vectorial form for convenience:

$$m \frac{d\vec{V}}{dt} = \Sigma \vec{F} + m\vec{g} \quad (\text{A.1})$$

$$\frac{d\vec{H}}{dt} = \Sigma \vec{M} \quad (\text{A.2})$$

Given the definitions stated in chapter 1 we can write the expression of the angular momentum \vec{H} . Every axis perpendicular to the axis of symmetry of the body is a principal axis of inertia. Therefore, the angular momentum \vec{H} can be expressed as the sum of the angular momentum about \vec{x} and the angular momentum about any perpendicular axis:

$$\vec{H} = I_x p \vec{x} + I_y \left(\vec{x} \times \frac{d\vec{x}}{dt} \right) \quad (\text{A.3})$$

It is important to notice that during the entire process of derivation of the linearized equations of motion, the vector \vec{x} is specified relative to $[\vec{i}, \vec{j}, \vec{k}]$ instead of $[\vec{I}, \vec{J}, \vec{K}]$. Since $[\vec{i}, \vec{j}, \vec{k}]$ is a rotating reference system with respect to the Newtonian frame of reference, the following differentiation rule needs to be used:

$$\left[\frac{d\vec{Q}}{dt} \right]_{(N/S)} = \frac{d\vec{Q}}{dt} + \vec{\omega} \times \vec{Q} \quad (\text{A.4})$$

Where Q can be any vector quantity.

The two vectorial equations of motion Equation A.1 and Equation A.2 are then written in the expanded version Equation A.5 and Equation A.6:

$$\frac{d\vec{V}}{dt} = \dot{V}\vec{i} + V \frac{d\vec{i}}{dt} = \frac{-\rho S C_D V^2}{2m} \vec{i} + \frac{\rho S C_{L_a} V^2}{2m} [\vec{i} \times (\vec{x} \times \vec{i})] - g \cos \phi \vec{j} \quad (\text{A.5})$$

$$\begin{aligned} I_x \dot{p} \vec{x} + I_x p \frac{d\vec{x}}{dt} + I_y \left(\vec{x} \times \frac{d^2 \vec{x}}{dt^2} \right) + I_y \frac{d\vec{\omega}}{dt} - I_y \left(\frac{d\vec{\omega}}{dt} \cdot \vec{x} \right) \vec{x} - 2I_y (\vec{\omega} \cdot \vec{x}) \frac{d\vec{x}}{dt} \\ + I_x p (\vec{\omega} \times \vec{x}) - I_y (\vec{\omega} \cdot \vec{x}) (\vec{\omega} \times \vec{x}) = \frac{1}{2} \rho S d V^2 \left(\frac{p d}{V} \right) C_{l_p} \vec{x} \\ + \frac{1}{2} \rho S d C_{M_a} V^2 (\vec{i} \times \vec{x}) + \frac{1}{2} \rho S d V^2 \left(\frac{p d}{V} \right) C_{M_{pa}} [\vec{i} - (\vec{i} \cdot \vec{x}) \vec{x}] \\ + \frac{1}{2} \rho S d^2 C_{M_q} V \left(\vec{x} \times \frac{d\vec{x}}{dt} \right) + \frac{1}{2} \rho S d^2 C_{M_a} V \left[\vec{x} \times \left(\frac{d\vec{x}}{dt} - \frac{d\vec{i}}{dt} \right) \right] \end{aligned} \quad (\text{A.6})$$

A.0.1 Linear Velocity Equation of Motion

By taking the dot product of both side of Equation A.5 with the unit vector \vec{i} :

$$\dot{V} = -\frac{\rho S C_D}{2m} V^2 \quad (\text{A.7})$$

Introducing the concept of "starred coefficients" as

$$C_x^* = \frac{\rho S d}{2m} C_x \quad (\text{A.8})$$

where C_x is a generic aerodynamic coefficient. We also change the independent variable from time to dimensionless distances through:

$$s = \frac{1}{d} \int_0^t V dt \quad (\text{A.9})$$

$$V' = \left(\frac{dV}{ds} \right) \quad (\text{A.10})$$

$$\dot{V} = \frac{dV}{ds} \cdot \frac{ds}{dt} = \left(\frac{V}{d} \right) V' \quad (\text{A.11})$$

The Equation of Motion for the linear velocity reduces to:

$$V' = -C_D^* V \quad (\text{A.12})$$

Equation A.12 is a first order differential equation, the solution of which is given by:

$$V = V_0 e^{\int_0^s -C_D^* ds} \quad (\text{A.13})$$

A.0.2 Roll Equation of Motion

The equation describing the roll motion can be easily decoupled from the yaw/pitch motion by taking the dot product of \vec{x} with Equation A.6:

$$\dot{p} = k_x^{-2} \left(\frac{V}{d} \right)^2 \left[\left(\frac{pd}{V} \right) C_{l_p}^* \right] \quad (\text{A.14})$$

where we define $k_x^{-2} = \frac{md^2}{I_x}$. Analogously $k_y^{-2} = \frac{md^2}{I_y}$. By recalling that the roll/spin rate p is the time derivative of the roll angle φ :

$$p = \frac{d\varphi}{dt} \quad (\text{A.15})$$

$$\dot{p} = \frac{d^2\varphi}{dt^2} \quad (\text{A.16})$$

By substituting this definition in Equation A.14 and changing independent variable to the dimensionless distance:

$$\phi'' + K_p \phi' = 0 \quad (\text{A.17})$$

where $K_p = -[k_x^{-2} C_{l_p}^* + C_D^*]$. The solution of Equation A.17, which is a linear second order differential equation, is:

$$\phi = \phi_0 - \frac{\phi'_0}{K_p} (e^{-K_p s} - 1) \quad (\text{A.18})$$

To obtain the solution in terms of spin/roll rate we just differentiate Equation A.17 with respect to non-dimensional distance s :

$$p = \frac{V}{d} \left(\frac{pd}{V} \right)_0 e^{-K_p s} \quad (\text{A.19})$$

Where the subscript "0" means that the quantity appearing in the expression is computed with the starting state values (usually the ones at the muzzle).

A.0.3 Linearized Yawing and Pitching Equation of Motion

We need to write the full Yawing and Pitching Equation of Motion with respect to the angle of attack α and the sideslip angle β , which are the representative angles of pitch and yaw respectively in this linearized framework. To do so we write the vector \vec{x} as the sum of its components in the rotating $[\vec{i}, \vec{j}, \vec{k}]$ frame:

$$\vec{x} = \cos \alpha \cos \beta \vec{i} + \sin \alpha \cos \beta \vec{j} + \sin \beta \vec{k} \quad (\text{A.20})$$

but since we are in a linearized framework (we assume that the yaw is small) Equation A.20 reduces to:

$$\vec{x} = \gamma \vec{i} + \alpha \vec{j} + \beta \vec{k} \quad (\text{A.21})$$

where $\gamma = \cos \alpha \cos \beta \approx 1$.

Taking advantage of Equation A.21, substituting Equation A.14 into Equation A.6 and changing the independent variable from time to dimensionless length we can obtain the 3 components of the equations for yawing and pitching motion:

i-component

$$(\beta'' - C_D^* \beta') \alpha - (\alpha'' - C_D^* \alpha') \beta + (P + 2G\beta) \gamma' + (P + G\beta) G\alpha = k_x^{-2} P C_{M_{p\alpha}}^* (1 - \gamma^2) + k_y^{-2} C_{M_q}^* (\alpha \beta' - \beta \alpha') + k_y^{-2} C_{M_{\alpha}}^* (\alpha \beta' - \beta \alpha' + G\alpha) \quad (\text{A.22})$$

j-component

$$(\gamma'' - C_D^* \gamma') \beta - (\beta'' - C_D^* \beta') \gamma + (P + 2G\beta) \alpha' \quad (\text{A.23})$$

$$+ \gamma (P + G\beta) (C_{L_\alpha}^* \alpha - G) - C_{L_\alpha}^* \beta' = -k_y^{-2} C_{M_\alpha}^* \beta - k_x^{-2} P C_{M_{p\alpha}}^* \gamma \alpha \quad (\text{A.24})$$

$$+ k_y^{-2} C_{M_q}^* (\beta \gamma' - \gamma \beta') + k_y^{-2} C_{M_\alpha}^* [\beta \gamma' - \gamma \beta' + \gamma (C_{L_\alpha}^* \beta - G)] \quad (\text{A.25})$$

k-component

$$(\alpha'' - C_D^* \alpha') \gamma - (\gamma'' - C_D^* \gamma') \alpha + (P + 2G\beta) \beta' \quad (\text{A.26})$$

$$+ \gamma (P + G\beta) C_{L_\alpha}^* \beta + C_{L_\alpha}^* \alpha' = k_y^{-2} C_{M_\alpha}^* \alpha - k_x^{-2} P C_{M_{p\alpha}}^* \gamma \beta \quad (\text{A.27})$$

$$+ k_y^{-2} C_{M_q}^* (\gamma \alpha' - \alpha \gamma') + k_y^{-2} C_{M_\alpha}^* (\gamma \alpha' - \alpha \gamma' - \gamma C_{L_\alpha}^* \alpha) \quad (\text{A.28})$$

The above equations can be considerably simplified through the linearization process. We neglect all the terms of higher order, namely:

- Products of α or β with γ' and γ''
- Products and squares of α and β
- Products with the derivates of α and β
- Products and squares of starred coefficients

The last group of negligible terms comes from the classical size assumptions often made in exterior ballistics. In our framework (small yaw assumption) the angles α and β are of order $[10^{-1}]$. The relative density factor $(\rho S d / 2m)$ is of order $[10^{-5}]$, which makes the largest starred coefficients of order $[10^{-3}]$. However we retain the product of P with starred coefficients since for large spin rates it can be of the same order of α and β .

By neglecting the previous listed groups of terms the i -component equation vanishes completely. We are left with two equations:

$$-\beta'' - C_D^* \beta' + P\alpha' - PG + PC_{L_\alpha}^* \alpha - C_{L_\alpha}^* \beta' = -k_y^{-2} C_{M_\alpha}^* \beta \quad (\text{A.29})$$

$$\begin{aligned} & -k_x^{-2} PC_{M_{p\alpha}}^* \alpha - k_y^{-2} (C_{M_q}^* + C_{M_{\dot{\alpha}}}^*) \beta' \\ & \alpha'' - C_D^* \alpha' + P\beta' + PC_{L_\alpha}^* \beta + C_{L_\alpha}^* \alpha' = k_y^{-2} C_{M_\alpha}^* \alpha \\ & -k_x^{-2} PC_{M_{p\alpha}}^* \beta + k_y^{-2} (C_{M_q}^* + C_{M_{\dot{\alpha}}}^*) \alpha' \end{aligned} \quad (\text{A.30})$$

To obtain the definitive linearized Yawing and Pitching Equation of Motion we need to adopt the complex notation, which is mathematically convenient to describe the geometric motion we want to study. By taking the product of the imaginary unit $-i = -\sqrt{-1}$ with Equation A.29, and summing it to Equation A.30 we get:

$$\begin{aligned} & (\alpha'' + i\beta'') - C_D^* (\alpha' + i\beta') + P (\beta' - i\alpha') + PC_{L_\alpha}^* (\beta - i\alpha) \\ & + C_{L_\alpha}^* (\alpha' + i\beta') + iPG = k_y^{-2} C_{M_\alpha}^* (\alpha + i\beta) - k_x^{-2} PC_{M_{p\alpha}}^* (\beta - i\alpha) \\ & + k_\gamma^{-2} (C_{M_q}^* + C_{M_{\dot{\alpha}}}^*) (\alpha' + i\beta') \end{aligned} \quad (\text{A.31})$$

We can now introduce the complex variable $\xi = \alpha + i\beta$ to obtain the final result:

Yaw and Pitch Equation

$$\xi'' + (H - iP)\xi' - (M + iP T)\xi = -iPG \quad (\text{A.32})$$

where

$$\begin{aligned} H &= C_{L_\alpha}^* - C_D^* - k_y^{-2} (C_{M_q}^* + C_{M_{\dot{\alpha}}}^*) \\ P &= \left(\frac{I_x}{I_y} \right) \left(\frac{pd}{V} \right) \\ M &= k_y^{-2} C_{M_\alpha}^* \\ T &= C_{L_\alpha}^* + k_x^{-2} C_{M_{p\alpha}}^* \\ G &= \frac{gd \cos \phi}{V^2} \end{aligned} \quad (\text{A.33})$$

Appendix B

Equations used in bulletStability code

All the equations and relations used in the `bulletStability` code are listed below:

$$\begin{aligned}
V &= V_0 e^{\int_0^s -C_D^* ds} \\
p &= \frac{V}{d} \left(\frac{pd}{V} \right)_0 e^{-K_p s} \\
\xi &= K_F e^{i\phi_F} + K_S e^{i\phi_S} + i\beta_R \\
\alpha &= \Re(\xi) \\
\beta &= \Im(\xi) \\
\alpha_{tot} &= \sqrt{\alpha^2 + \beta^2} \\
K_F &= K_{F_0} e^{\lambda_F s} \\
K_S &= K_{S_0} e^{\lambda_S s} \\
\phi_F &= \phi_{F_0} + \phi'_{F'} \\
\phi_S &= \phi_{S_0} + \phi'_{S'} \\
\beta_R &= \frac{PG}{M + iPT} \\
\phi'_F &= \frac{1}{2} \left[P + \sqrt{P^2 - 4M} \right] \\
\phi'_S &= \frac{1}{2} \left[P - \sqrt{P^2 - 4M} \right] \\
\lambda_F &= -\frac{1}{2} \left[H - \frac{P(2T - H)}{\sqrt{P^2 - 4M}} \right] \\
\lambda_S &= -\frac{1}{2} \left[H + \frac{P(2T - H)}{\sqrt{P^2 - 4M}} \right] \\
K_{F_0} e^{i\phi_{F_0}} &= \left(\frac{i\xi'_0 + \phi''_S \xi_0}{\phi'_F - \phi'_S} \right) \\
K_{S_0} e^{i\phi_{S_0}} &= \left(\frac{i\xi'_0 + \phi''_F \xi_0}{\phi'_F - \phi'_S} \right) \\
H &= C_{L_\alpha}^* - C_D^* - k_y^{-2} \left(C_{M_q}^* + C_{M_{\dot{\alpha}}}^* \right) \\
P &= \left(\frac{I_x}{I_y} \right) \left(\frac{pd}{V} \right) \\
M &= k_y^{-2} C_{M_\alpha}^* \\
T &= C_{L_\alpha}^* + k_x^{-2} C_{M_{p\alpha}}^* \\
G &= \frac{gd \cos \phi}{V^2} \\
G_0 &= \frac{gd \cos \phi}{V_0^2} \\
\varepsilon &= \sqrt{1 - 1/S_g} \frac{\sin \delta_{max}}{\left(2 \frac{I_y}{I_x} - 1 \right)} \\
\xi_0 &= (\sin \varepsilon) e^{i\varphi_0} \\
\xi'_0 &= i \left(\frac{pd}{V} \right) (\sin \varepsilon) e^{i\varphi_0}
\end{aligned}$$

$$\begin{aligned}
J_A &= -i \left[\left(\frac{2\pi}{n} \right) (k_y^2 - k_x^2) \left(\frac{C_{L_\alpha}}{C_{M_\alpha}} \right) \sin \varepsilon \right] e^{i\varphi_0} \\
T_L &= i \left[\left(\frac{2\pi}{n} \right) \left(L_N + \frac{1}{2} L_{CYL} - XCG \right) \sin \varepsilon \right] e^{i\varphi_0} \\
D_R &= ik_y^2 \left(\frac{PG_0}{2} \right) \left(\frac{C_{L_\alpha}}{C_{M_\alpha}} \right) s^2 \left[1 + \frac{2}{3} (C_D^* s) + \frac{1}{3} (C_D^* s)^2 \right]
\end{aligned}$$

Appendix C Results from the simulations

Table C.1: Initial conditions and results for the 9x19mm Parabellum 124gr

Quantity	Symbol	Starting Value	Final Value	Unit
Mass	m	8.03	-	[g]
Rifling Twist Rate	n	1/9.84	-	[turn/inches]
In-Bore Yaw	ε	0.96	-	[°]
Maximum Downrange	S_{max}	100	-	[m]
Initial Roll Angle	φ_0	0	-	[°]
Maximum First Yaw	δ_{max}	5	-	[°]
Spin Rate	p	86221	76139	[RPM]
Speed	V	360	286.7	[m/s]
Mach number	Ma	1.04	0.84	[‐]
Gyroscopic Stability Factor	S_g	9.46	11.345	[‐]
Dynamic Stability Factor	S_d	0.51	0.61	[‐]
Final Total Angle of Attack	α_{tot}	-	0.55	[°]
Yaw of Repose	β_R	0.019	0.033	[°]
Aerodynamic Jump Deflection	J_{Ad}	0	15.4	[cm]
Lateral Throw-off Deflection	T_{Ld}	0	0.152	[cm]
Drift	D_R	0	2.14	[cm]
Total Deflection	Def	0	17.4	[cm]

Table C.2: Initial conditions and results for the 9x19mm Parabellum 158gr

Quantity	Symbol	Starting Value	Final Value	Unit
Mass	m	10.23	-	[g]
Rifling Twist Rate	n	1/9.84	-	[turn/inches]
In-Bore Yaw	ε	0.57	-	[°]
Maximum Downrange	S_{max}	100	-	[m]
Initial Roll Angle	φ_0	0	-	[°]
Maximum First Yaw	δ_{max}	5	-	[°]
Spin Rate	p	76556	71938	[RPM]
Speed	V	318.9	282.4	[m/s]
Mach number	Ma	0.92	0.82	[‐]
Gyroscopic Stability Factor	S_g	5.66	6.38	[‐]
Dynamic Stability Factor	S_d	0.49	0.54	[‐]
Final Total Angle of Attack	α_{tot}	-	1.19	[°]
Yaw of Repose	β_R	0.022	0.030	[°]
Aerodynamic Jump Deflection	J_{Ad}	0	11.5	[cm]
Lateral Throw-off Deflection	T_{Ld}	0	0.09	[cm]
Drift	D_R	0	1.82	[cm]
Total Deflection	Def	0	13.2	[cm]

Table C.3: Initial conditions and results for 9x39mm SP-5 subsonic bullet

Quantity	Symbol	Starting Value	Final Value	Unit
Mass	m	16.1	-	[g]
Rifling Twist Rate	n	1/8.3	-	[turn/inches]
In-Bore Yaw	ε	0.21	-	[°]
Maximum Downrange	S_{max}	400	-	[m]
Initial Roll Angle	φ_0	0	-	[°]
Maximum First Yaw	δ_{max}	5	-	[°]
Spin Rate	p	85381	75307	[RPM]
Speed	V	300	251.4	[m/s]
Mach number	Ma	0.87	0.73	[‐]
Gyroscopic Stability Factor	S_g	2.38	2.62	[‐]
Dynamic Stability Factor	S_d	0.175	0.206	[‐]
Final Total Angle of Attack	α_{tot}	-	2.28	[°]
Yaw of Repose	β_R	0.019	0.029	[°]
Aerodynamic Jump Deflection	J_{Ad}	0	8.29	[cm]
Lateral Throw-off Deflection	T_{Ld}	0	0.003	[cm]
Drift	D_R	0	6.73	[cm]
Total Deflection	Def	0	15.0	[cm]

Table C.4: Initial conditions and results for 7mm bullet

Quantity	Symbol	Starting Value	Final Value	Unit
Mass	m	10	-	[g]
Rifling Twist Rate	n	1/7.3	-	[turn/inches]
In-Bore Yaw	ε	0.05	-	[°]
Maximum Downrange	S_{max}	300	-	[m]
Initial Roll Angle	φ_0	0	-	[°]
Maximum First Yaw	δ_{max}	5	-	[°]
Spin Rate	p	273552	255787	[RPM]
Speed	V	850	700	[m/s]
Mach number	Ma	2.45	2.02	[‐]
Gyroscopic Stability Factor	S_g	1.26	1.58	[‐]
Dynamic Stability Factor	S_d	0.38	0.38	[‐]
Final Total Angle of Attack	α_{tot}	-	1.83	[°]
Yaw of Repose	β_R	0.0027	0.004	[°]
Aerodynamic Jump Deflection	J_{Ad}	0	13.0	[cm]
Lateral Throw-off Deflection	T_{Ld}	0	0.026	[cm]
Drift	D_R	0	1.78	[cm]
Total Deflection	Def	0	14.8	[cm]